

Development of NiTiCu Shape Memory Alloy by Directed Energy Deposition Processes

M.Tech. Thesis

By

Prasanna Santosh Bairagi



**Department of Mechanical Engineering
Indian Institute of Technology Indore**

May 2024

Development of NiTiCu Shape Memory Alloy by Directed Energy Deposition Processes

A THESIS

*Submitted in partial fulfilment of the
requirements for the award of the degree
of*
Master of Technology

by
Prasanna Santosh Bairagi



**Department of Mechanical Engineering
Indian Institute of Technology Indore**

May 2024



Indian Institute of Technology Indore

CANDIDATE'S DECLARATION

I hereby certify that the work which is being presented in the thesis entitled **Development of NiTiCu Shape Memory Alloy by Directed Energy Deposition Processes** in the partial fulfilment of the requirements for the award of the degree of **Master of Technology** and submitted in the **Department of Mechanical Engineering, Indian Institute of Technology Indore**, is an authentic record of my own work carried out during the time period from **July 2022** to **May 2024** under the supervision of **Dr. Dan Sathiaraj** (Associate Professor) and **Prof. Neelesh Kumar Jain** (Professor, HAG) of Department of mechanical Engineering, Indian Institute of Technology Indore

The matter presented in this thesis has not been submitted by me for the award of any other degree of this or any other institute.

Bairagi

Prasanna Santosh Bairagi

This is to certify that the above statement made by the candidate is correct to the best of our knowledge.

Dan Sathiaraj

Dr. Dan Sathiaraj

Neelesh Kumar Jain

Prof. Neelesh Kumar Jain

Prasanna Santosh Bairagi has successfully given his M.Tech. Oral Examination held on **3rd June 2024**.

Neelesh Kumar Jain

Signature(s) of Supervisor(s) of M.Tech. thesis

Date: *07/06/2024*

Dan Sathiaraj

D. Jaisankar

Convener, DPGC

Date: *07/06/24*

Acknowledgements

I take this opportunity to express my deep sense of respect and gratitude to **Dr. Dan Sathiaraj** and **Prof. Neelesh Kumar Jain** for believing in me to carry out this work under their supervision. Their constant encouragement, friendly interactions and constructive support have enabled this work to achieve its present form. Their innovative perspective towards things and his continuous pursuit for perfection has had a profound effect on me and has transformed me majorly. I am very thankful from the depth of my heart to committee members for their precious guidance and support. Their active attention in my research and valuable discussions have compelled me to dive deeper and deeper in my research work and thus helped me immensely to bring this research to its present form. I am also thankful to all the faculties of our Mechanical Engineering Department for their support and allowing me to use their lab facilities without which I would not be able to carry a single step forward in my research.

I am greatly thankful and convey my special gratitude to the Head of Department of Mechanical Engineering and DPGC convener for supporting and providing us facilities, their moral support and friendly nature throughout my M. Tech program. The services of the staff, Discipline of Mechanical Engineering, IIT Indore are acknowledged with sincere thanks. It is a pleasure to acknowledge the support and help extended by **Miss Poonam Deshmukh, Mr. Pradyumn Arya and Mr. Rajendra Goud** for their guidance and support.

I cannot close these prefatory remarks without expressing my deep sense of gratitude and reverence to my dear parents and my friends for their blessings and Endeavour to keep my moral high throughout the period of my work. I want to express my sincere thanks to all those who directly or indirectly helped me at various stages of this work.

Prasanna Santosh Bairagi

DEDICATION

This thesis is dedicated to my father, who taught me that hard work and perseverance are the keys of success. It is also dedicated to my mother, who taught me that even the largest task can be accomplished if you keep faith in yourself. It is also dedicated to my supervisor who was the guiding light every step of the way as I researched for this dissertation.

Abstract

Alloys possessing super-elasticity and shape memory effect are referred to as shape memory alloys (SMAs). They are used for a wide range of applications including actuators, micro-electro-mechanical systems (MEMS), and biomedical implants. NiTi (commonly known as Nitinol) is the most commonly used SMA. But it suffers from the limitations of relatively narrow working temperature range and high hysteresis loss. Adding copper to NiTi alloy to form NiTi_xCu SMAs addresses these limitations by reducing the hysteresis temperature thus enhancing functional lifespan and thermal stability of the resultant SMA. This improvement is crucial for those applications that require precise thermal control and consistent performance over time. Therefore, objectives of present research are: (i) Development of multi-layer deposition of NiTi₂₀Cu SMA from the wires of NiTi and Cu by the twin wire arc additive manufacturing (T-WAAM) process using the identified optimum parameters from its single-layer single-track depositions manufactured during the main experiments, (ii) Development of multi-layer depositions of NiTi, NiTi₅Cu and NiTi₂₀Cu using powders of Ni, Ti and Cu by the micro-plasma arc metal additive manufacturing (μ -PAMAM) process using the identified optimum parameters from their single-layer single-track depositions manufactured during the main experiments. Objective is to study the effect of varying amount of Cu in NiTi on mechanical properties and shape memory effect, (iii) Characterization of multi-layer depositions of NiTi, NiTi₅Cu, and NiTi₂₀Cu using microstructure, chemical composition, formation of phases, tensile properties, microhardness, phase transformations to illustrate shape memory effect, and (iv) Comparative study of NiTi, NiTi₅Cu, and NiTi₂₀Cu using their characterizations. The experimental investigations were performed in the following three stages: (i) *pilot experiments* to bracket the ranges of variable process parameters and to identify values of the fixed parameters for both T-WAAM and μ -PAMAM processes, (ii) *main experiments* manufacturing single-track single-layer depositions of NiTi_xCu SMAs by T-WAAM and μ -PAMAM processes using one factor at a time approach for both the processes. The objective was to identify their optimum parameters for multi-layer depositions, and (iii) multi-layer depositions of NiTi_xCu SMAs by T-WAAM and μ -PAMAM processes using their identified optimum parameters.

Incorporation of copper was found to significantly influence the microstructure and mechanical properties of the developed NiTi₅Cu and NiTi₂₀Cu. Specifically, it improved their microhardness and tensile strength more robust and durable. Phase transformation behaviour of developed NiTi_xCu SMAs demonstrated reduction in hysteresis temperature implying that they can make transition between the phases more efficiently. This will be beneficial for their applications in actuators and MEMS where rapid and reliable responses to temperature changes are essential. Overall, this study provides valuable insights into the fabrication and optimization of NiTi_xCu SMAs by direct energy deposition (DED) type additive manufacturing processes using their constituents in both wire and powder forms. Findings of the present work contribute to broader understanding of development of NiTi_xCu SMAs and enhancing their properties, functionality, and overall performance thus opening up new possibilities for their applications in high-tech and critical applications across various fields.

Table of Contents

Item	Page No.
Acknowledgment	vii
Dedication	ix
Abstract	xi
List of Figures	xv
List of Tables	xvii
Abbreviation	
Chapter 1: Introduction	1-14
1.1 Shape Memory Alloys	1
1.1.1 Advantages of Shape Memory Alloys	2
1.2 Shape Memory Effect	4
1.3 Bulk Deposition of NiTi and NiTiCu	6
1.4 Additive Manufacturing	7
1.4.1 Classification of AM Processes	7
1.4.2 Advantages, Limitations, Applications of AM Processes	8
1.5 Directed Energy Deposition (DED) Processes	11
1.5.1 Types of DED Processes	11
1.5.2 Advantages, Limitations, and Applications of DED Processes.....	12
1.5.3 Suitability of DED Processes for SMAs	13
1.6 Organization of Thesis	14
Chapter 2: Review of Past Work	15-23
2.1 Effect of Cu Addition to NiTi	15
2.2 Development of NiTi and NiTiCu by Different Processes	17
2.3 Development of NiTi by Additive Manufacturing	17
2.4 Summary of Literature Review	20
2.5 Identified Research Gaps	21
2.6 Research Objectives	21
2.7 Research Methodology.....	21
Chapter 3: Details of Experimentation	25-34
3.1 Deposition of NiTi _x Cu SMAs by μ -PAMAM Process	24
3.1.1 Materials for μ -PAMAM Process	24
3.1.2 Machine for μ -PAMAM Process	25
3.1.3 Pilot and Main Experiment for μ -PAMAM Process	27
3.1.4 Multi-layer Deposition of NiTi _x Cu by μ -PAMAM Process	28

3.2 Deposition of NiTi20Cu SMA by T-WAAM Process	28
3.2.1 Materials for T-WAAM Process	28
3.2.2 Machine for T-WAAM Process	29
3.2.3 Pilot and Main Experiment for T-WAAM Process	30
3.2.4 Multi-layer Deposition of NiTi20Cu by T-WAAM Process	31
3.3 Measurement of the Responses	32
3.3.1 Aspect Ratio and Dilution	32
3.3.2 Microstructure and Chemical Composition	33
3.3.3 Evolution of Phases	33
3.3.4 Tensile Testing	33
3.3.5 Microhardness Evaluation	34
3.3.6 Transformation of Phases	34
Chapter 4: Results and Discussions	35-53
4.1 Characteristics of Single-layer Depositions	35
4.1.1 Single-layer Depositions by μ -PAMAM Process	35
4.1.2 Single-layer Depositions by T-WAAM Process	38
4.2 Optimized Multi-layer Depositions of NiTi _x Cu SMAs	40
4.3 Analysis of Microstructure and Chemical Composition	41
4.4 Analysis of Evolution of Phases	46
4.5 Microhardness Results	48
4.6 Tensile Properties	49
4.7 Phase Transformation Behaviour	51
Chapter 5: Conclusions and Scope for Future Work	55-57
5.1 Significant Achievements	55
5.2 Conclusions	55
5.3 Scope for Future Work	57
References	59-63

List of Figures

Figure Number and Captions	Page No.
Fig.1.1: Application of Shape memory alloys.....	3
Fig.1.2: Concept of hysteresis loop in an SMA.....	4
Fig.1.3: Phase transformations in an SMA phases and corresponding crystal structures.....	5
Fig.1.4: Classification of AM.....	8
Fig. 3.1: Morphology of powder particles of NiTi20Cu alloy.....	25
Fig.3.2: Working principle of μ -PAMAM process.....	25
Fig.3.3: Photograph of 5-axis CNC machine developed for μ -plasma metal additive manufacturing (μ -PAMAM) process.....	26
Fig.3.4: Machine for T-WAAM process: (a) schematic diagram, and (b) photograph.....	30
Fig.3.5: Location of different samples from the optimized multi-layer deposition along its the build direction for evaluation of different responses.....	32
Fig.3.6: Schematic view of single-layer deposition (where, ' W ' is deposition width; ' H ' is deposition height; ' AR ' is aspect ratio; ' D ' is dilution; ' P ' is diluted area; ' Q ' is deposition area).....	33
Fig. 4.1: Photographs of single-layer deposition of NiTi5Cu by μ -PAMAM process: (a) uniform continuous deposition, and (b) non-uniform continuous deposition.....	36
Fig. 4.2: Photographs of single-layer depositions of NiTi20Cu SMA fabricated by T-WAAM process: (a) Uniform continuous depositions, and (b) Nonuniform continuous depositions.....	38
Fig. 4.3: Optimized multi-layer deposition of NiTi _x Cu SMA manufactured by μ -PAMAM process: (a) NiTi, (b) NiTi5Cu, and (c) NiTi20Cu.....	41
Fig. 4.4: Optimized multi-layer deposition of NiTi20Cu SMA fabricated by T-WAAM process.....	41
Fig. 4.5: Microstructure, elemental mapping, and chemical composition of optimized multi-layer depositions for: (a1 and a2) μ -PAMAM manufactured NiTi SMA, (b1 and b2) μ -PAMAM manufactured NiTi5Cu SMA, (c1 and c2) μ -PAMAM manufactured NiTi20Cu, and (d1 and d2) T-WAAM manufactured NiTi20Cu SMA.....	45

Fig. 4.6: XRD graphs for multi-layer depositions of NiTi, NiTi5Cu, and NiTi20Cu by μ -PAMAM process and NiTi20Cu by T-WAAM process.....	47
Fig. 4.7: Results of microhardness evaluation of NiTi _x Cu SMAs: (a) microhardness profile along the build direction, and (b) average values of microhardness.....	48
Fig. 4.8: Tensile test results of NiTi _x Cu alloys: (a) NiTi, (b) NiTi5Cu, (c)NiTi20Cu by μ -PAMAM process and (d)NiTi20Cu by T-WAAM process.....	50
Fig. 4.9: Phase transformation pattern of NiTi _x Cu alloys: (a) NiTi, (b) NiTi5Cu, (c)NiTi20Cu by μ -PAMAM process and (d)NiTi20Cu by T-WAAM process.....	52

List of Tables

Table No.	Page No.
Table 2.1: Research methodology used in the present work to meet the identified research objectives.....	23
Table 3.1: Chemical composition of the prepared powders of NiTi _x Cu SMA for their depositions by μ -PAMAM process.....	24
Table 3.2: Values of μ -PAMAM process parameters used in different phases of experiments.....	27
Table 3.3: Values of T-WAAM process parameters used in different phases of experiments.....	30
Table 4.1: Measured and computed responses for single-layer deposition of NiTi ₅ Cu SMA by μ -PAMAM process for different combinations of μ -plasma power and deposition head travel speed.....	36
Table 4.2: Measured and computed responses for single-layer deposition of NiTi ₂₀ Cu SMA by T-WAAM process for various combinations of voltages and deposition head travel speed.....	39
Table 4.3: Chemical composition (by wt.%) of multi-layer depositions of NiTi- _x Cu alloys obtained from their EDS spectrum.....	46
Table 4.4: Ultimate tensile strength (UTS) and elongation for the optimized multi-layer depositions of NiTi _x Cu SMAs obtained from their tensile tests.....	50

Abbreviation

A_f	Austenite Finish
AM	Additive manufacturing
A_s	Austenite Start temperature
ASTM	American Society for Testing and Materials
ASTM	American Society for Testing and Materials
CMT	cold metal transfer
DED	Direct energy deposition
DLP	digital light processing
DSC	differential scanning calorimetry
EBAM	electron beam additive manufacturing
EBM	electron beam melting
EB-PBF	electron beam powder bed fusion
FGM	functionally graded materials
GMA	gas metal arc
JCPDS	Joint Committee on Powder Diffraction Standards
LENS	Laser engineering net shape
LMD	laser metal deposition
LOM	laminated object manufacturing
MEMS	micro-electromechanical systems
M_f	Martensite Finish
M_s	Martensite Start
MTT	martensitic transformation temperature
NCD	non-uniform continuous deposition
PAAM	plasma arc additive manufacturing

PAD	plasma arc deposition
PBF	Powder Bed Fusion
SLA	stereolithography
SMA	Shape memory alloys
SME	shape memory effect
T-WAAM	twin wire arc additive manufacturing
TWSME	two-way SME
UAM	Ultrasonic additive manufacturing
UCD	uniform continuous deposition
WAAM	wire-arc additive manufacturing
WSEM	wire spark erosion machining
XRD	x-ray diffraction
μ-	micro-plasma arc metal additive manufacturing
PAMAM	

Chapter 1

Introduction

1.1 Shape Memory Alloys (SMA)

Shape memory alloys (SMA) have become the most promising and first-choice material for different actuators and/or sensor applications in the devices based on micro-electromechanical systems (MEMS). Any actuation mechanism in a smart system is governed by the controlled production of work output or energy release. The principle behind the SMA actuators is the conversion of thermal energy into kinetic energy and work output. The SMA actuators offer large range of motion at low operating voltages. An array of benefits, such as high recoverable forces, large recoverable output strains up to (8%), different actuation mode (linear, bending, torsion), and high work output per unit volume or mass, can be achieved by the SMA actuators. Therefore, SMA actuators have become one of the most preferred choices. They are being widely used in performing different actuation functions in various applications, for example, as the thin films in functioning of micro-pumps and micro-valves and as the bulk material for adaptive wing structure and thermos-variable springs due to their maverick characteristics of super-elasticity and thermal shape memory effect (**Leng et al., 2007, Wu et al., 2008, Li et al., 2009**). The SMAs have some limitations also such as poor response behavior, large thermal energy loss and limited temperature ranges. Many researchers are trying to improve their capabilities to enhance their usefulness in other technological applications.

The SMA deforms it into a predefined shape in a controlled way because it has two phases at different temperatures. The first is the low temperature martensite phase and second is the high temperature austenite phase. These phase transformations can be obtained only if the constituents of an alloy are blended perfectly under proper lattice arrangements leading to the *shape memory effect* (SME). The SME is observed for many alloys including NiTi, Cu-Al-Ni, Cu-Zn-Al, Cu-Sn, Nb-Ti, Cu-Al-Be, Ag-Cd, Au-Cd, Fe-Mn-Si, Fe-Pt and Ti-Nb. Out of the SMAs mentioned above, only two alloy systems, NiTi and copper-based alloys and their combination with minute quantities of dopants have promising technology advantages. The other alloys are not suitable for industrial applications because either the constituent elements are too expensive or they cannot be used as SMA unless they are in the form of single crystals (**Pons, 2005 and Liang, 1990**).

Though SME was observed in early 1950s but engineering importance of SMAs was not recognized till the equi-atomic NiTi alloy was synthesized in 1963 in the Naval Ordnance Lab (NOL) was named as 'Nitinol' which has name of its chemical constituents and its

synthesizers i.e., Ni (Nickel) + Ti (Titanium) + nol (**Otsuka, 1998, Moberly and Melton, 1990**). During last 4 decades, binary NiTi alloys have been intensively investigated to cater functional applications. NiTi based SMAs have emerged as the most important commercial SMAs because of their unique shape-memory performance, stability of retaining SME, prolong fatigue life, maverick nature of getting adapted almost under all the environments, ease of processing, pseudo-elasticity and possession of the required mechanical properties (**Pons, 2005 and Liang, 1990**). Additionally, they exhibit excellent corrosion resistance and biocompatibility enabling development of biomedical implants from NiTi. The inter-metallic NiTi₂ compounds are extra-ordinary because they have moderate solubility range for excess of nickel or titanium, as well as with other metallic elements. This solubility allows, alloying possibility with many other elements, to modify both the mechanical and phase transformation characteristics. These materials have exhibited some exciting application potential in MEMS, biomedical implants, intelligent materials and structural systems, either in the monolithic form or in combination with other materials. Consequently, binary alloy NiTi has an edge over all the remaining SMA due to its tailor-made smart structures from NiTi have successfully been developed for a variety of applications.

However, NiTi has its own limitation such as relatively narrow working temperature range and high hysteresis loss which sequentially reduces the life of the NiTi product. Adding copper to NiTi alloy to form ternary alloy NiTiCu as SMA addresses these limitations by reducing the hysteresis temperature and at the same exhibiting an equal amount of efficient actuation similar to that NiTi thus enhancing functional lifespan and thermal stability of the resultant SMA. This improvement is crucial for those applications that require precise thermal control and consistent performance over time. Compared with NiTi binary alloy, NiTiCu alloys shows less composition sensitivity in transformation temperatures lower martensitic yield stress, and superior fatigue property which makes them more suitable for micro actuator application

1.1.1 Advantages and Applications of SMAs

Use of SMA based actuators and systems have emerged as a very promising alternative to replace the existing conventional actuators and systems due to their following advantages:

- **Mass and volume savings:** SMA actuators have the potential capability to achieve high output/weight ratio as compared to the traditional actuators.
- **Minimum system complexity:** SMA actuators are always associated with spring structures. Therefore, need of dampers and overall system complexity of structures can be minimized.
- **Retraction capability:** usually it is available only in motor-type structures.

- **Noiseless operation:** SMA actuators remove the vibration disturbance to other payloads that are normally associated with motor-driven deployment.
- **Sensing capability:** Both actuating and sensing functions can be combined by measuring changes in the electrical resistance associated with the phase transformation.
- **Higher reliability:** The movement is triggered by a phase transformation and the speed of movement is related to the temperature of the SMA element, which is determined by the thermal input and heat transfer. Therefore, it is possible to design systems with large torque margins.
- **Large recoverable strains:** SMA actuators permits use of extremely long strokes and the application of large forces when deformation is restrained.
- **High electrical resistivity:** It means that the shape transformation can be activated by passing an electrical current through a SMA elements, thus avoiding the need of the separated heaters.
- **Design Flexibility:** SMA actuators can be linear, rotary, or combination of both, and can form an integral part of a component. Thus, it appears that SMS-actuators can combine practically all the advantages of controlled and free-movement.

SMA's are being used for different applications in various fields. Their some major applications are shown in Fig. 1.1.

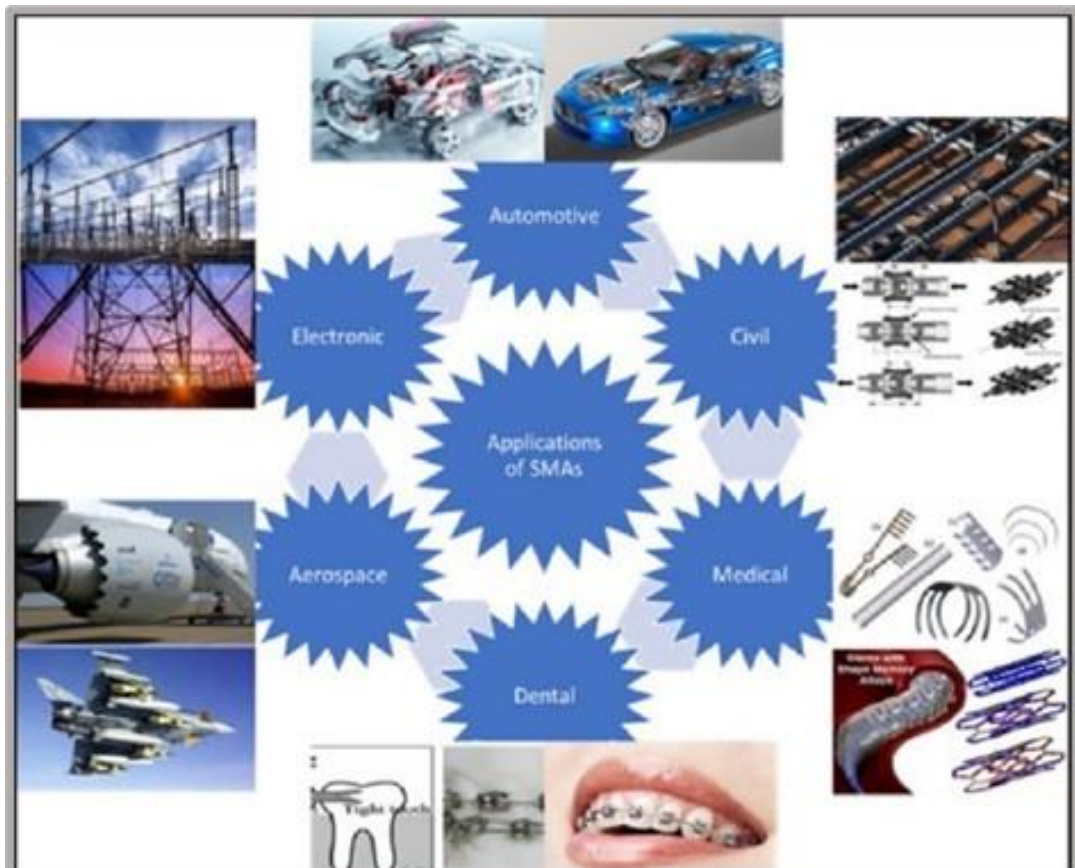


Fig.1.1: Application of Shape memory alloys (Raza et. al., 2021)

1.2 Shape Memory Effect

The SMAs can sustain large amount of strain without any permanent deformation. This strain can be recovered either by changing the temperature or the load causing SMAs to return back to their original shape. This is known as the shape memory effect (SME) i.e., restoring the original shape from a plastically deformed shape. It occurs due to transition from one crystal structure to another and this phenomenon is known as *thermo-elastic martensitic transformation*. The SME of SMAs is caused due the phase transformations (martensite to austenite and vice versa) which is initiated either due to change in temperature or applied load. If the phase transformation occurs due to change in temperature (i.e., heating or cooling), then it is known as *temperature induced phase transformation*. If phase transformation is caused by change in stress, then it is known as *stress induced phase transformation*. It occurs at a constant temperature which is moderately more than the austenite finish temperature leading to super-elasticity effect. It can be summarized that a reversible solid state phase transformation, known as *martensitic transformation*, is the main driving force behind functioning of the SMAs. Phase transformation cycle of a SMA has following characteristics temperatures as shown in Fig.1.2:

1. Austenite Start ' A_s '
2. Austenite Finish ' A_f '
3. Martensite Start ' M_s '
4. Martensite Finish ' M_f '

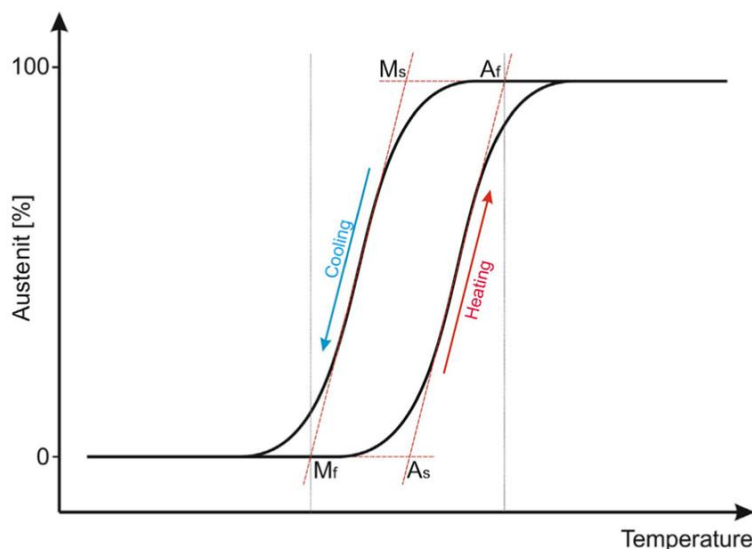


Fig. 1.2: Concept of hysteresis loop in an SMA (Andrianesis et al., 2007).

The heating process of a SMA evolves the austenite phase when temperature reaches ' A_s ' and the transformation process is completed when the temperature reaches ' A_f '. Whereas, during the cooling process, formation martensite phase start at temperature ' M_s ' and is

completed at the temperature ' M_f '. The difference between transition temperatures is called hysteresis. The transformation from the austenite to martensite and the reverse transformation from the martensite to austenite do not take place at the same temperature. The characteristics temperatures are in the order of $M_f < M_s < A_s < A_f$.

As discussed earlier the application of SMA are widely used as actuators in the MEMS applications. The primary requirement for being an actuator is the ability of material to function with high frequency and fast response. Low hysteresis and narrow range of transformation temperatures help in becoming an efficient actuation. The phase transformation temperatures of an SMA can be evaluated by the differential scanning calorimetry (DSC). It provides an insight into SMAs unique characteristics such as one-way effect, two-way effect, hysteresis, super-elasticity, and rubber elasticity. It explains thermal and mechanical effects on the SME. It is a good tool to perform calculations on the thermal implications of the stress induced phases transformation. It also explains the reversibility of the phase transition in certain SMAs and highlights energy contributions that controls the hysteresis phenomenon (Peng et al., 2008). An SMA can have one-way and two-way SME as explained below and shown in Fig. 1.3.

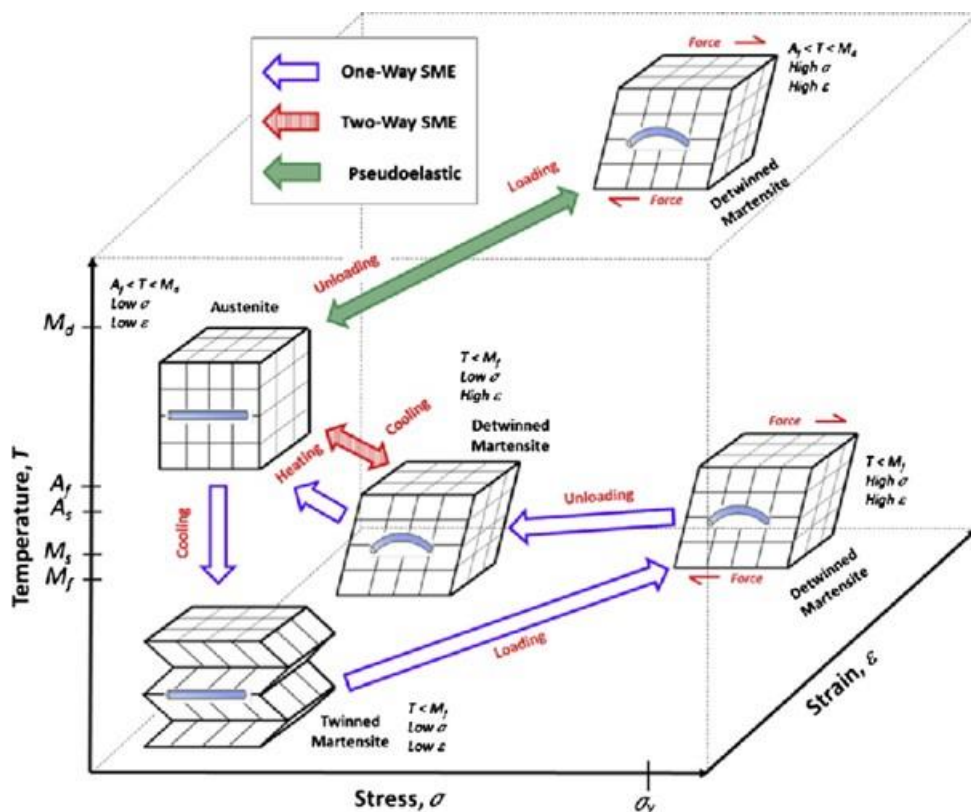


Fig. 1.3: Phase transformations in an SMA phases and corresponding crystal structures (Mohd Jani et al., 2014)

- **One-Way SME:** An SMA exists in martensite phase at a temperature below ' M_f '. In this condition, it is soft and can be deformed quite easily by detwinning as shown in Fig. 1.3. This deformation involves movement of highly mobile twin boundaries. Heating the SMA up to ' A_f ' converts it to the austenite phase and the specimen reverses to its original shape and no additional shape change take place during the cooling (**Tadaki et al., 1988**). Therefore, this effect is called 'one way SME' and it can be repeatedly induced by deforming SMA in the martensitic state. The shape change start at ' A_s ' and gets completed at ' A_f ' which is a small temperature range i.e., 10 to 30K.
- **Two-Way SME:** The SMAs with two-way SME (TWSME) remembers both its shapes at high temperature phase (i.e., austenite) and the low temperature phase shape (martensite). The recoverable strain in such SMAs is usually about half of those SMAs having one-way SME. Following methods can be used to induce specific mechanical/thermal treatments in a SMA to produce two-way SME: (a) SME training through temperature cycling, (b) induce severe deformation in the martensitic state, (c) combined training, (d) forces of inactive surface layers. Temperature cycling can be used for training the NiTi SMA since it has sufficient ductility.

1.3 Bulk Deposition of NiTi and NiTiCu SMAs

Recent progress in research, in the fabrication of SMAs, has open new ways to develop noble actuators and systems, which are capable of performing smart functions by responding to their thermal, mechanical and magnetic environment in a controlled manner. Most commercial applications of SMAs can be grouped into the following three categories: (i) shape memory actuation devices, (ii) super-elastic devices and (iii) martensitic devices. Shape memory actuation devices utilize the shape memory effect and can be further sub-divided into the following three groups: (a) free recovery, (b) constraint recovery, and (c) partially constraint recovery. Super-elastic devices use the phenomenon of super-elasticity and provide a constant force over large strains. They exhibit larger torque and larger kink resistance. Martensite devices employ the deformation of SMA material in the martensite phase and result in very high damping characteristics and remarkable fatigue strength. They can be easily deformed plastically while, strains can be recovered on heating.

NiTi and NiTiCu SMAs have been developed for a broad range of applications in the field of aerospace, industrial and biomedical applications. This has been realized because of their low manufacturing cost, good corrosion resistance, biocompatibility and tailored material properties. Their applications in aerospace include fabrication of elevators, transportation of large sophisticated equipment and quick connect-disconnect couplings. Their industrial applications include connectors and fasteners, couplings, tweezers,

monolithic micro-grippers, robotic actuators, micromanipulators, and gas flow control valves. In bio-medical field these are being used for orthodontic arch wires, blood clot filters, orthopedic implants, stents, and bone anchor.

1.4 Additive Manufacturing

Additive manufacturing (AM) is a revolutionary manufacturing philosophy process in which three-dimensional objects are created by adding the material layer by layer. Unlike traditional subtractive manufacturing processes where material is removed from a solid block to create the final shape, additive manufacturing builds objects using bottom-up approach thus offering greater design flexibility and efficiency. An AM process begins with a digital 3D model of the product to be manufactured. This model is sliced into thin horizontal layers using specialized software. Each layer is then sent to the AM machine which follows the instructions to deposit the material according to the product design. The deposition or feedstock material could be polymer, metal and alloys, ceramic, composites, bio-polymers, or even construction materials depending on the specific application.

1.4.1 Classification of AM Processes

According to ASTM F42, different AM processes are categorized into the following seven categories as shown in Fig 1.4:

- **Powder Bed Fusion (PBF) Processes:** This type processes involve spreading a thin layer of powder metallic or polymeric material onto a build platform and then selectively melting or sintering the powder with a laser or electron beam. Selective laser sintering (SLS), selective laser melting (SLM), direct metal laser sintering (DMLS), and selective heat sintering (SHS) are common AM processes in this category, with each differing in terms of the materials used and the level of melting involved.
- **Directed Energy Deposition (DED) processes:** use a focused energy source such as a laser beam, electron beam, and suitable arc to melt material as it is deposited. This process is often used for repairing or adding material to existing components and for producing large-scale objects with metallic alloys. Laser engineering net shape (LENS), laser metal deposition (LMD), wire-arc additive manufacturing (WAAM),
- **Sheet Lamination Processes:** Sheet lamination involves bonding together sheets of of same material or different materials, typically metal foil or paper, using heat, adhesive, or ultrasound waves as the energy source. Layers are cut to shape using a laser or blade, and each layer is then bonded to the previous one until the object is fully formed. Ultrasonic additive manufacturing (UAM), and laminated object manufacturing (LOM) are examples of this category.

- **Material Extrusion Processes:** This process involves extruding material through a nozzle to build up layers. Common materials used include thermoplastics and thermoplastic composites. Layers are typically deposited onto a build platform, with the nozzle moving in the x and y axes while the platform moves in the z-axis to build up the a product layer by layer.
- **Vat Polymerization Processes:** Use a photopolymer resin which is cured by a light source, typically a laser or projector, to create solid layers. It includes stereolithography (SLA) and digital light processing (DLP). The build platform starts at the bottom of a vat of liquid resin. A light source selectively cures the resin according to the cross-section of the product being built, solidifying each layer as it moves upward.
- **Material Jetting Processes:** Material jetting is similar to inkjet printing but they use materials such as photopolymers or waxes instead of ink. These materials are jetted onto a build platform and cured layer by layer. The jetting heads move across the build platform, depositing droplets of material according to the digital design, and are then cured or solidified by UV light.
- **Binder Jetting Processes:** In binder jetting, a liquid binding agent is selectively deposited onto a powder bed, binding the particles together to form the solid layers. Once a layer is completed, the build platform lowers, and a new layer of powder is spread on top. This process continues until the entire object is formed.

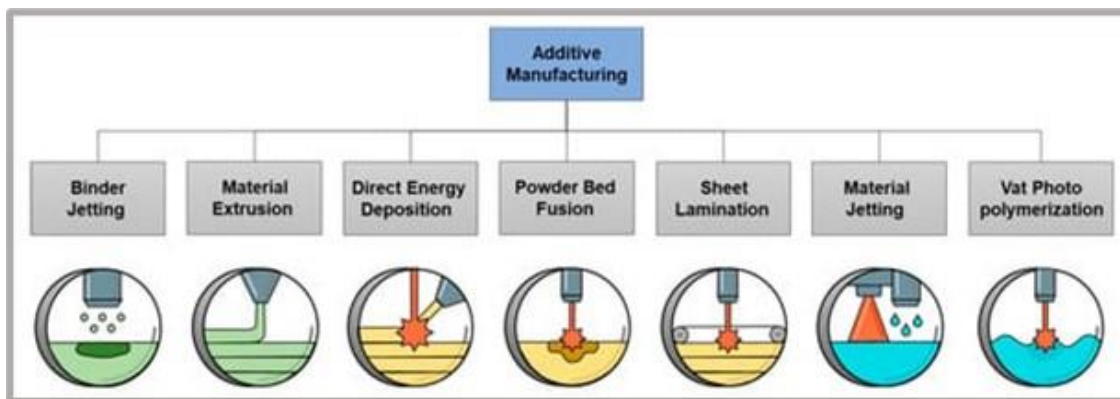


Fig.1.4: Classification of AM processes according to ASTM F42 (Ron et al., 2023)

1.4.2 Advantages, Limitations, Applications of AM Processes

Following are some unique advantages offered by AM processes:

- **Free-form fabrication:** Additive Manufacturing (AM) transcends the boundaries of traditional manufacturing processes such as casting, powder metallurgy, forming, and machining. It enables the production of parts having intricate geometries.

- **Digital Driven Fabrication:** AM processes are driven by computer programs therefore they can accurately manufacture optimized complex geometries. This high level of control ensures repeatability and precision in produced parts.
- **Controllable Multi-Material Production:** AM supports the development of functionally graded materials, smart materials, and biomaterials by utilizing multiple materials in the desired proportions, enhancing the ability to create advanced materials.
- **Minimization of Assembly Requirements:** Layered deposition of the materials in the AM processes enables manufacturing of a complicated assembly without need to manufacture its components individually. This minimizes the requirement of assembly which improves reliability of the manufactured product.
- **Cost-Effective Personalized Manufacturing:** Unlike traditional large-scale production that requires costly and time-consuming molds, AM processes can directly transform a CAD model into a physical object without the need for a mold. This efficiency is beneficial for applications such as multi-functional surgical tools, customized bone replacements, and heritage replication and repair.
- **Automated Manufacturing Process:** The ability of AM to create complex geometries and use multiple materials allows for the automated production of intricate and material-diverse objects using a single machine, minimizing the need for human intervention.
- **Material Waste Reduction:** Traditional manufacturing often involves removing material from a larger dimension which can result in significant wastage of the material. AM on the other hand builds parts from scratch by adding material thus ensuring minimal waste and reducing the need for tooling.
- **Environmental Advantages:** AM offers significant environmental benefits over traditional manufacturing. It is more material efficient and energy efficient thus contributing to a more sustainable manufacturing process. By using the necessary material to create a part, AM minimizes the environmental impact associated with waste products.

Although AM process offers many significant advantages but they still suffer from the following limitations.

- **Material Constraints:** AM machines are typically designed to work with a limited range of materials that possess similar properties. Processing different materials on a single AM machine is challenging due to varying reshaping processes. Advancements in material science are crucial for the broader realization of AM technology.
- **Extended Production Time for Large-Scale Manufacturing:** While AM excels in creating customized products, it is generally suited for small-scale production. AM

processes are often employed to produce complex geometries that are difficult to achieve with traditional manufacturing methods.

- **Limited Manufacturing Accuracy:** The layer-by-layer manufacturing approach of AM processes compromises with dimensional and geometrical accuracy and surface finish of the manufactured product. Sometimes curved surfaces of a manufactured product does not precisely match the intended surfaces.
- **Need for Post-Processing:** AM processes are not net-shape manufacturing processes but serve as a primary step in the production cycle. Components produced via AM often require additional post-processing to achieve the desired dimensional and geometrical accuracy and surface finish of a product.
- **Data Intensity for Complex Products:** Producing geometrically intricate products via AM involves handling large amounts of data. Developing efficient algorithms to manage this complexity remains a significant challenge.

Since the late 1980s, AM processes have been advancing technology, gaining widespread use over the past decade. The transformative applications of AM have significantly impacted the following industries:

- **Biomedical:** AM processes are transforming the biomedical sector by enabling the production of functional prototypes, surgical-grade components, and lifelike anatomical models. Innovations include orthopaedic implants, dental devices, and a range of tools and instrumentation such as seamless medical carts, customized saw and drill guides, and bespoke surgical tools. The development of certified biocompatible materials is crucial, potentially revolutionizing customized implants, life-saving devices, and pre-surgical tools.
- **Aerospace:** The aerospace industry was an early adopter of AM benefiting from the need for its high-performance, flight-worthy components. The AM applications in aerospace include environmental control system ducting, customized aircraft interior components, rocket engine parts, and combustor liners. AM allows for the creation of complex, consolidated parts with enhanced strength, reduced material usage, and lower weight.
- **Consumer Products:** AM is utilized by marketing teams, designers, and graphic artists to quickly bring their ideas to market, simulating the final product look and feel. AM has proven valuable for consumer goods such as sporting equipment and electronics, enabling detailed iterations early in product development. As AM technology continues to evolve, it is expected to meet larger volume demands in the consumer products market.
- **Energy:** The energy sector benefits from AM processes due to their ability to rapidly produce customized components and environmentally friendly materials that can endure

extreme conditions. Key applications include control-valve components, pressure gauge pieces, turbine nozzles, rotors, flow meter parts, and pump manifolds. AM also holds potential for creating specialized parts for underwater or harsh environment use.

- **Transportation:** AM has allowed the transportation industry to develop lightweight components capable of withstanding extreme speeds and heat while minimizing the drag. Some applications include complex ductwork, durable prototypes, customized interior features, grilles, and large panelling.

1.5 Directed Energy Deposition (DED) Processes

The DED type AM processes hold significant importance in the realm of AM due to their unique capabilities and advantages. They offer unparalleled versatility in material selection, allowing for the deposition of a wide range of materials, including metals, alloys, ceramics, and composites. It makes them highly adaptable to diverse applications across various industries. Moreover, DED processes typically boast high deposition rates, enabling faster build rates as compared to other AM processes, particularly when depositing large volumes of a material. This increased productivity reduces overall production time, making DED processes an attractive option for industries with demanding production schedules. One of the standout features of DED processes is their suitability for repair and cladding applications. The ability to add material to existing components for repair or reinforcement purposes is invaluable in those industries where equipment downtime must be minimized, such as aerospace, oil and gas, and automotive sectors. Additionally, DED processes can be easily scaled up to accommodate the fabrication of large-scale components and structures, making them well-suited for applications requiring the production of sizable parts. In terms of design flexibility, DED processes offer the engineers and designers significant freedom to create complex geometries and customized parts with intricate features. This flexibility enables the production of innovative solutions tailored to specific requirements, fostering creativity and pushing the boundaries of what is achievable in manufacturing. Furthermore, DED processes are known for their material efficiency because they only add the material where it is needed thus reducing material wastage and associated costs as compared to other AM processes and the traditional manufacturing processes. This aspect aligns with sustainability goals and makes the DED processes environmentally friendly manufacturing option.

1.5.1 Types of DED Processes

- **Laser-based DED processes:** utilize a high-power laser beam as the heat source to melt and deposit metallic powder or wire onto a substrate. In this method, the laser beam is precisely controlled and directed towards the substrate surface, where it melts the feedstock material allowing it to fuse with the substrate or previously deposited layers.

Laser-based DED processes offer exceptional precision and control over the deposition process, enabling the fabrication of complex geometries with high accuracy. This technique is widely used in industries such as aerospace, automotive, and tooling for rapid prototyping, repair of the damaged components, and near-net manufacturing of the parts.

- **Electric arc-based DED processes:** also known as wire arc additive manufacturing (WAAM) processes, employs an electric arc (i.e., manual metal arc, gas metal arc, gas tungsten arc,) as the heat source to melt and deposit metal wire onto a substrate. In this process, an electric arc is generated between a metallic wire as the feedstock material and the substrate surface, creating intense heat that melts the wire as it is deposited onto the substrate. The WAAM processes offer high deposition rates and is suitable for producing large components with low-cost materials. They are commonly used in industries such as aerospace and marine for manufacturing structural components and large-scale parts where speed and cost-effectiveness are crucial.
- **Plasma-based DED process:** often referred to as plasma arc additive manufacturing (PAAM) utilize a plasma arc as the heat source to melt and deposit metal powder or wire onto a substrate. In these processes, a plasma arc is generated by passing a gas, typically argon or nitrogen, through a high-voltage electrical arc, creating a high-temperature plasma jet. This intense heat melts the feedstock material which is then deposited onto the substrate surface to build up the part. They offer high deposition rates and excellent metallurgical properties, making them suitable for the applications requiring high-performance components in industries such as aerospace, defence, and energy.

1.5.2 Advantages, Limitations and Applications of DED Processes

Advantages: One of the primary advantages of DED processes is their versatility in material selection. They can deposit a wide range of materials, including metals, alloys, ceramics, and composites offering flexibility for diverse applications. They also allow for the deposition of materials with different properties in a single build thus enabling development of functionally graded materials (FGM), SMA, biocompatible materials, smart materials having tailored mechanical, thermal, or electrical properties. The DED processes offer high deposition rates, particularly WAAM and PAAM processes. It makes them suitable for producing large-size components efficiently, reducing overall production time and costs. They have excellent design flexibility allowing for the fabrication of complex geometries with intricate features. This capability enables the engineers and designers to create innovative solutions and customized parts tailored to a specific requirement. The DED

processes can also be used for repair and cladding applications, extending the lifespan of critical components and reducing maintenance costs.

Limitations: Despite their numerous advantages, the DED processes also have some limitations that need attention. One limitation is the problem of residual stresses and distortion in manufactured parts, particularly in the DED processes involving high-energy sources such as laser beam or plasma arc. Proper design and process optimization are necessary to mitigate these effects and ensure dimensional accuracy and quality of the produced parts. The requirement for post-processing operations such as machining, grinding, lapping or heat treatment processes to achieve the desired surface finish, dimensional and geometrical accuracy, and surface texture. These additional steps increase production time and costs although advancements in process monitoring and control are helping to minimize the need for extensive post-processing.

Applications: The DED processes find applications across various industries, including aerospace, automotive, defence, oil and gas, chemical, dies and molds, and tooling. In aerospace industries, the DED processes are used for manufacturing complex structural components, engine parts, and repair of turbine blades. In automotive industries, they are employed for rapid prototyping, rapid tooling, and customization of the parts. In defence sector, they are utilized for manufacturing lightweight armour, missile components, and repair of military vehicles. In the oil and gas industry, the DED processes are used for producing wear-resistant coatings, repair of drilling equipment, and downhole tools. In tooling and mould making industries, DED processes enable the fabrication of inserts, cores, and cavity components having intricate features.

1.5.3 Suitability of DED Processes for SMA

The DED processes present unique advantages for the fabrication of SMA components, offering precise control over the deposition process and enabling the production of complicated geometries with tailored properties. SMAs require specific processing conditions to preserve their unique characteristics of shape memory effect. Therefore, DED processes are particularly suitable for fabricating components from SMAs due to the following reasons:

- DED processes provide excellent control over the local thermal history during deposition, minimizing the risk of phase transformations and preserving the SME of an SMA. This precise control ensures that the SMA retains its shape memory properties allowing it to recover its original shape when subjected to the appropriate thermal stimulus.
- DED processes allow for deposition of SMA in a controlled environment reducing the risk of oxidation and contamination which could adversely affect properties of an SMA. The design flexibility offered by DED enables the fabrication of complex SMA

components with tailored mechanical properties such as stiffness, ductility, and shape memory behaviour.

- DED processes offer possibility of depositing SMA onto an existing component for repair or modification purposes extending the lifespan of SMA-based devices and systems. This capability is particularly beneficial in industries such as aerospace, automotive, and biomedical where SMA components are subjected to harsh operating conditions and may require periodic maintenance or refurbishment.
- Several studies have highlighted the advantages of using DED processes for fabricating components from SMAs. For example, research conducted by **Wang et al. (2021)** demonstrated the feasibility of fabricating complex SMA structures by DED process with precise control over the deposition and excellent shape memory behaviour. Studies by **Ma et al. (2023)** and **Guo et al. (2021)** explored use of DED processes for producing SMA-based actuators and biomedical implants respectively highlighting their capabilities.

1.6 Organization of the Thesis

This thesis is organized into the following five chapters:

- Chapter 1** mentions introduction of SMA, SME, bulk deposition of NiTi and NiTiCu SMAs, classification of additive manufacturing processes, types, advantages, limitations and applications of DED processes, and suitability of DED processes for shaping SMAs.
- Chapter 2** provides review of the relevant past work on development of NiTi and NiTiCu by conventional processes and additive manufacturing processes, effect of copper addition to NiTi, identified research gaps, and research objectives of the present work and methodology used to meet them.
- Chapter 3** describes preparation of powders to develop NiTi_xCu by μ -PAMAM process by mixing 5at.% and 20at.% of Cu with powders of Ni and Ti, machines for μ -PAMAM and T-WAAM process, details of experimentations by μ -PAMAM and T-WAAM process, preparation of samples and procedure for evaluation of aspect ratio, dilution, microstructure, evolution of phases, tensile properties, phase transformation behaviour of the developed SMAs.
- Chapter 4** presents the results for the single-layer and optimized multi-layer depositions of NiTi_xCu SMAs and NiTi₂₀Cu SMA fabricated by μ -PAMAM and T-WAAM process respectively, results and analysis for aspect ratio and dilution of the single-layer depositions, and analysis of microstructure, formation of phases, tensile properties, microhardness, and phase transformation behaviour for optimized multi-layer depositions.
- Chapter 5** Summarizes the outcome of the present research by presenting its significant achievements, conclusions, and some directions for the future work.

Chapter 2

Review of Past Work

2.1 Effect of Cu Addition to NiTi

Goryczka and Humbeeck (2008) fabricated NiTiCu SMAs by *powder metallurgy* which required precise adjustments in temperature and duration of sintering to achieve the uniform SMAs. For the SMA containing less than 5 at% of copper and 50 at% of titanium, sintering temperature of 940°C and sintering duration of 7 hours yielded homogeneous SMA with regular transformation properties. Whereas, for the SMA having more than 10 at% of copper required sintering temperature of 850°C and 20 hours of sintering duration to produce the homogeneous SMA. Despite the developed SMAs having less than 25% inherent porosity, their reversible martensitic transformation closely resembled to that of dense SMAs.

Shiva et. al., (2016) used *laser rapid manufacturing* process to add copper to NiTi SMA and performed comprehensive characterizations of the resultant SMAs. Their investigations focused on particle structure, phase transformations, and shape memory effects. Laser rapid manufacturing process proved to effective for fabricating NiTiCu25 SMA while maintaining its shape memory properties. Comparable characteristics were observed between NiTi50 and NiTiCu25 SMAs. Study of microstructure and chemical composition exhibited satisfactory quality and phase analysis indicated phase transformation peaks in NiTiCu25. Results of DSC confirmed phase transformations in both NiTi50 and NiTiCu25 SMAs.

Fu et. al. (2018) found that the microstructure of *laser-cladded* NiTi and NiTiCu coatings exhibits a notable change from coarse crystal grains near the fusion line to island structures and dendrites towards the surface, signifying a variation in phase ratios. Copper addition predominantly impacted the grain boundary regions of the matrix, fostering the formation of a NiTiCu ternary phase. This study highlights the considerable alteration in coating properties due to Cu inclusion. Despite a modest decrease of only 3.9°C in the ' M_s ' temperature, there is a substantial 100% enhancement in hardness changing from 300-400HV to 650-700HV. Additionally, friction properties improve with 25.8% reduction in friction coefficient and approximately 50% decrease in the wear loss. These enhancements stem from grain boundary reinforcement and the wetting effect induced by the intergranular ternary phase, coupled with alterations in phase transformation behaviour.

Velmurugan and Senthilkumar (2018) investigated influence of adding copper to nanocrystalline NiTi SMA by *high-energy ball milling* process for a duration 30 hours. It facilitated formation of nanocrystalline intermetallic based on NiTi and NiTiCu. Copper addition significantly reduced crystal size of NiTiCu SMA as compared to that of NiTi SMA

which led to enhanced lattice strain. High-energy ball milling process transformed lamellar structure of NiTi based intermetallic into a homogenized fine granular structure of NiTiCu based intermetallic which led to reduction in its particle size. Formation of slender shaped particles in NiTiCu SMA after the ball milling process increased its hardness by 31%. Summarily, this study advocates Cu addition by mechano-synthesis process for a duration of 30 hours to achieve well-ordered microstructure and mechanical properties of NiTiCu SMA.

Santosh and Sampath (2020) developed NiTi_xCu SMAs by varying at.% of copper content from 2, 4, 6, 8, 10 via *vacuum induction melting* process and tailored their thermo-mechanical processing to optimize their properties. Their analysis using the CHNOS software confirmed that carbon and oxygen impurities (which are known to degrade SMA performance) were within the acceptable limits in all the SMAs. Their phase analysis validated the successful alloying with presence of prominent austenite peaks and faint martensite peaks. The DSC revealed that inclusion of copper increased nearly all transformation temperatures with evidence of two-step transformation in some SMAs. Hardness of the developed SMAs showed steady increase with increase in copper content which is attributed to the formation of Cu-rich precipitates. Microstructure examination revealed needle-like martensite dispersed within an austenitic matrix.

Salman (2021) manufactured four wires of NiTi, NiTi₂Cu, NiTi₅Cu, NiTi₈Cu SMAs by the *casting* process and studied effect of varying copper content to NiTi SMA on microstructure, phase transformations, and electrical conductivity. Microscopic examination revealed homogeneous distribution of all the elements within the SMAs. Study of microstructure found presence of austenite and martensite phases, and manufacturing defects. The DSC results elucidated phase transformations between austenite and martensite phases. Assessment of SME found that Ni₅₂Ti₄₀Cu₈ SMA has the best shape memory retention. Hardness and electrical conductivity of the developed SMAs increased with the copper content and Ni₅₂Ti₄₀Cu₈ SMA has the higher hardness and electrical conductivity than the other SMAs. His findings underscore multifaceted impact of SMA composition on its microstructure, mechanical properties, and electrical conductivity which can contribute to optimization of their wire manufacturing process.

Cirstea et al. (2023) used *spark plasma sintering* process to develop $Ti_{50}Ni_{50-x}Cu_x$ SMAs and studied of influence of their microstructure on their mechanical properties. They highlighted hardening potential of phases of TiNiCu SMAs through formation of ternary compounds of Ti, Ni, and Cu. Rapid temperature increase and high cooling rates led to formation of $Ti_2(Ni, Cu)$ and $(Ti, Cu) Ni_3$ intermetallic compounds within the TiNiCu matrix. Mechanical indentation analysis found influence of stable TiNiCu, Ni, or Ti phases and precipitates of $Ti(Ni, Cu)_2$ phase. Vicker's microhardness of 350 HV and elastic modulus around 75 GPa.

2.2 Development of NiTi and NiTiCu by Different Processes

Following processes have been used for development NiTi SMA: solid-state sintering, hot extrusion, hot pressing, hot isostatic pressing (**Morries et al., 1989**), pulse laser deposition (**Gu et al., 1998**), powder metallurgy (**Bram et al. 2002, Valeanu et al. 2011**), field activated pressure assisted synthesis (**Locci et al., 2003**), plasma melting and metal injection molding (**Araújo et al. 2011**). But, these processes have been successfully used to manufacture thin films of NiTi SMA for deploying it development in various functional devices particularly actuators for various MEMS applications especially in micro-pumps and micro-valves. Detailed characterization has been done for the developed thin films. But development of bulk structures of NiTi SMA by these processes has not been probed by the researchers.

Following is the summary of different processes used for development of NiTiCu SMA: **Goryezka et al. (2001)** manufactured ribbons of NiTiCu SMA by hot rolling assisted melt spin process. **Hassdorf et al. (2002)** manufactured thin film of NiTiCu SMA by molecular beam epitaxy process. **Cai et al. (2007)** deposited thin film of NiTiCu SMA by magnetron sputtering on various flexible substrates and glass substrates. **Mineta et al. (2007)** fabricated cylindrical micro-actuator by etching of TiNiCu SMA. **Araujo et al. (2011)** used hot rolling assisted vacuum plasma melting process for NiTiCu as well as NiTi. **Alijani et al. (2014)** demonstrated manufacturing of NiTiCu through mechanical alloying via ball milling process.

2.3 Development of NiTi by Additive Manufacturing

Kubasova et al., (2024) carried out review of different DED and PBF type AM processes used for production of NiTi SMA. This review paper explains about electron beam powder bed fusion (EB-PBF) process, pioneered by Arcam AB under the trade name of electron beam melting (EBM), in addition to other AM process. EBM process uses a high-power electron beam to melt the feedstock material powder to create a 3D object. This electron beam is generated by accelerating electrons in a vacuum environment. This makes EBM process ideal for NiTi SMAs and all those materials that are susceptible to contamination from oxygen and other airborne chemicals. EBM process utilizes a system

with powder hoppers, a rake, and a printing platform similar to SLM process. Researchers have tried to understand impact of vacuum chamber temperature on EBM-fabricated NiTiS SMA and reported that a preheating temperature of 450°C avoids both powder ignition and insufficient bonding. However, this approach can lead to exothermic reactions due to the use of elemental Ni and Ti powders. Following paragraphs present review of different type of AM process used for development of bulk parts from NiTi SMA by different researchers during the last two decades.

Krishna et al. (2007) used *laser net shape engineering* (LENS) process for bulk deposition of NiTi SMA and investigated impact of process parameters on the depositions. They found that increasing laser power or powder feed rate led to larger grain size. Higher energy densities, achieved through increased laser power or slower scan speeds, yielded denser parts with reduced porosity which improved compressive strength of NiTi SMA.

Lu et al. (2018) used *plasma arc deposition* (PAD) process for manufacturing NiTi SMA studied its microstructure, phase transformations, and mechanical properties. Their investigation found that the microstructure varied throughout the deposition of SMA showing cellular structure at the bottom, dendritic structure in the middle, and equiaxed structure at the top. They attributed this variation to the temperature gradient during solidification. Additionally, formation of irregular Ti_2Ni phase was observed due to a specific reaction during solidification. This phase interacted with the surrounding TiNi matrix influencing NiTi SMA two-step phase transformation upon cooling. Interestingly, the as-deposited NiTi parts exhibited favourable properties such as high hardness and strength, and a unique quasi-linear super-elasticity with a narrow hysteresis loop achieving up to 3.8% strain recovery.

Sujith et al. (2019) used *LENS* process for deposition of NiTi SMA and studied effect of process parameters on microstructure, mechanical behaviour, pseudo-elasticity of the developed SMA. They reported that laser energy density affects super-elastic behaviour of NiTi SMA and that its deposition fabricated at 20-50 J/mm² energy density exhibited excellent super-elasticity at low strain levels.

Wang et al. (2019) performed comparative of in-situ alloying and effects of process parameters on microstructural homogeneity, phase formation, and thermomechanical properties for NiTi SMA depositions produced by *SLM*, *laser-based DED* process, and *selective EBM* processes using pre-mixed powders of Ni and Ti. They found that the laser-based DED process produced good quality deposition of NiTi SMA having good interlayer fusion and phase transformation characteristics though formation of uniformly dispersed Ti_2Ni intermetallic can cause embrittlement. The SLM produced NiTi deposition had a balance between microstructural inhomogeneity and keyhole defects produced due to energy

density variations. This is due to strong exothermic reaction in mixture of powders of Ni and Ti during the SLM process which disrupts the melt pool and complicates formation of the desired phases. They found that SEBM process unsuitable for in-situ alloying of NiTi SMA due to lack-of-fusion in preheating and powder-ignition dilemma. This study suggests that DED is the more effective process for in-situ alloying of NiTi SMA when elementally blended powders is to be used as the feedstock material.

Dutkiewicz et al. (2020) compared martensitic transformation temperature (MTT) of the depositions of NiTi SMA made by *LENS* and *electron beam additive manufacturing* (EBAM) processes. They found that the LENS fabricated sample showed MTT at -26°C which is less than the raw powder. For the EBAM fabricated sample, the MMT reached at -19°C . The peaks of martensite and reverse transformations were diffused due to differences in grain size and composition across the samples. Aging treatment at 500°C for 2 hours not only separated R-phase during cooling of both the samples but also formed sharper and higher transformation peaks and increased their MTT.

Pu et al. (2021) used *wire-based vacuum additive manufacturing* process to fabricate depositions of NiTi SMA and studied microstructure, phase transformation, and tensile super-elasticity and found them to vary along the build direction of produced depositions. The as-built part had columnar grains and strong texture along the build direction. Top region of the as-built NiTi part showed lower phase transformation temperatures and better super-elasticity whereas, the middle and bottom regions exhibited higher phase transformation temperatures and poor super-elasticity. They reported that heat treatment can be used to adjust transformation behaviour and super-elasticity along the build direction. Their results prove that wire-based vacuum additive manufacturing is very promising process to produce dense and pure NiTi functional structures with good working condition adaptability.

Resnina et. al. (2021a) fabricated five layers of NiTi on a titanium substrate by the gas metal arc (*GMA*) based *WAAM* process using Ni-rich NiTi wire. The first layer showed dendritic Ti-rich NiTi phase and inter-dendritic Ti_2Ni phase due to re-melting of the titanium substrate. Subsequent layers exhibited columnar and equiaxed grains with varying chemical compositions in dendritic matrix and inter-dendritic space. Concentration of nickel increased from the first to fourth layer equalling to that of Ni-rich NiTi wire. Despite different compositions, all layers underwent B2 to B19 transformation with varied temperature ranges. Tensile tests conducted at room temperature revealed distinct deformation mechanisms across different layers, initiating with stress-induced martensite transformation in the third layer and progressing through subsequent layers. Analysis of SME confirmed recoverable deformation in the fabricated NiTi samples.

Liu et al. (2022) used cold metal transfer (*CMT*) based WAAM process to fabricate wall shaped components from TiNi SMA using optimized depositing speed and analyzed their microstructure, mechanical properties, and wear performance. They observed refinement of coarse columnar grains, and monotonic increase in microhardness, critical stress and elongation along the build direction, equiaxed microstructure in the upper region, and distribution of Ni₄Ti₃ precipitates in the matrix. They reported that plastic deformation combined with wear-induced work hardening is the main form of wear which is mainly hindered by the super-elasticity of NiTi SMA.

Singh et al. (2023) studied influence of interlayer temperature on porosity level, morphology, and mechanical characteristics of multi-layer depositions of NiTi SMA produced by *CMT based WAAM* process using 200°C, 400°C, and no interlayer temperature control. SME of the manufactured depositions was examined using hot plate actuation. Their findings demonstrate that regulating the interlayer temperature below 300°C (preferably at 200°C) enhances microstructure and mechanical characteristics and decreases porosity of NiTi walls. Though CMT based WAAM process with optimized depositing speed produced good homogeneity of microstructure, mechanical properties, and wear resistance indicating that this process has great potential to make novel flexible structures from NiTi SMA. However, compositional heterogeneity between layers and presence of a brittle Ti₂Ni phase remains the challenge as observed by **Resnina et al. (2021b)**. These inconsistencies impact super-elasticity and shape memory behaviour of the parts of NiTi SMA.

Fink et al. (2023) used *electron beam powder bed fusion* process fabricate Ti-rich, dense, and crack-free structures from NiTi SMA, analysed martensitic phase transition behaviour, studied segregation during the solidification through Thermo-calc simulation, and investigated one-way and two-way SME of the as-built NiTi parts. The fabricated NiTi parts showed microstructure having fine columnar grains and numerous precipitates. They studied their influence on the tensile properties at room temperature.

2.4 Summary of Literature Review

Additive manufacturing (AM) techniques offer promising methods for creating NiTi parts with tailored properties. The AM processes allow precise control over material deposition and process parameters, enabling the creation of complex NiTi structures with good mechanical properties. However, careful optimization of parameters is crucial to achieve fully dense parts with minimal microstructural inconsistencies and avoid challenges like residual stresses, surface roughness, and compositional variations. Addition of copper to NiTi SMA introduces several benefits. Studies have shown that it improves the tensile strength,

wear resistance, and electrical conductivity. It can also influence grain structure and phase transformation behaviour, leading to potentially superior shape memory properties.

2.5 Identified Research Gaps

Following are the research gaps identified from review of the relevant past work:

- Considerable work has been done on deposition of NiTi SMA using different AM processes.
- Different processes such as hot rolling assisted melt spin, molecular beam epitaxy, magnetron sputtering, etching, hot rolling assisted vacuum plasma melting, and ball milling have been used for making *thin films* of NiTiCu SMA.
- Very Limited work available on deposition of NiTiCu SMA by AM process.
- No work is available on bulk depositions of NiTiCu SMA using wire and powder forms of Ni, Ti, and Cu, and comparative study of NiTiCu SMA with NiTi SMA.

2.6 Research Objectives

Following are research objectives (RO) of the present work based on the identified research gaps:

- **RO-1:** Development of multi-layer deposition of NiTi20Cu SMA from the wires of NiTi and Cu by twin wire arc additive manufacturing (T-WAAM) process using the identified optimum parameters from single-layer depositions fabricated during main experiments.
- **RO-2:** Development of multi-layer depositions of NiTi, NiTi5Cu and NiTi20Cu from the powders of Ni, Ti and Cu by the micro-plasma arc metal additive manufacturing (μ -PAMAM) process using the identified optimum parameters from their single-layer depositions manufactured during the main experiments. Objective is to study effect of varying amount of Cu in NiTi on mechanical properties and shape memory effect.
- **For RO-1 and RO-2:** Characterization of multi-layer depositions of NiTi, NiTi5Cu, and NiTi20Cu using microstructure, chemical composition, formation of phases, tensile properties, microhardness, phase transformations to illustrate shape memory effect.
- **RO-3:** Comparative study of NiTi, NiTi5Cu, and NiTi20Cu using their characterizations.

2.7 Research Methodology

Table 2.1 presents the research methodology used in the present work to meet the identified research objectives. Experimental investigations were performed in the following three stages: (i) *pilot experiments* to bracket the ranges of variable process parameters and to identify values of the fixed parameters for both T-WAAM and μ -PAMAM processes, (ii) *main experiments* manufacturing single-layer depositions of NiTiCu SMAs by T-WAAM and μ -PAMAM processes using one factor at a time approach for both the processes to

identify their optimum parameters for the multi-layer depositions, and (iii) multi-layer depositions of NiTi_xCu SMAs by T-WAAM and μ -PAMAM processes using their identified optimum parameters.

This chapter presented review of the relevant literature, identified research gaps, research objectives of the present work along with the methodology used to meet them. The **next chapter** describes details related to different aspects of the experiments performed for depositions of NiTi_xCu SMAs by μ -PAMAM and T-WAAM processes.

Table 2.1: Research methodology used in the present work to meet the identified research objectives.

RO-1: Development of multi-layer depositions of NiTi, NiTi5Cu and NiTi20Cu SMAs by micro-plasma arc metal additive manufacturing (μ-PAMAM) process and their characterization:		
Stage of experimentation	Pilot experiments: To identify optimum values/ranges of μ -PAMAM process parameters for good and continuous deposition of NiTi5Cu alloy using a one-factor-at-a-time approach.	Main experiments [No. of experiments: 9]: To identify optimum values of the two variable parameters using criteria of the type of deposition, lower aspect ratio, and low % dilution
Input parameters and responses for single-layer depositions	Variable input parameters: μ -plasma power: 110-440 W; Mass flow rate of deposition material powder: 0.6-5.0 (g/min); Deposition head travel speed: 40-200 (mm/min); Flow rate of μ -plasma forming gas: 0.1-0.5 Normal liter per minute (NI/min); Flow rate of shielding gas: 3-8 (NI/min); Stand-off distance (SOD): 5-12 mm Response: Visual examination for continuous deposition	Variable input parameters: μ -plasma power: 363; 374; 385 W; Mass flow; Deposition head travel speed: 47; 51; 55 mm/min Constant input parameters: Flow rate of μ -plasma forming gas: 0.25 NI/min; rate of deposition material powder: 2.9 g/min; Flow rate of shielding gas: 4.5 NI/min; SOD: 8 mm Responses: Measurement of aspect ratio, % dilution visual examination for uniform and continuous deposition
Input parameters for multi-layer depositions of NiTi_xCu SMAs: Main experiments identified optimum values of 374 W for μ -plasma power and 51 mm/min for deposition head travel speed. This parametric combination was used to manufacture a 60 mm long multi-layer deposition from the prepared powders of NiTi, NiTi5Cu, NiTi20Cu alloys on Ti6Al4V base plate.		
RO-2: Development of multi-layer deposition of NiTi20Cu SMA by the twin wire arc additive manufacturing (T-WAAM) process and its characterization:		
Stage of experimentation	Pilot experiments: To identify optimum values/ranges of T-WAAM process parameters for good and continuous deposition of NiTi20Cu alloy using a one-factor-at-a-time approach.	Main experiments [No. of experiments: 12]: To identify optimum values of the three variable parameters using criteria of the type of deposition, lower aspect ratio
Input parameters and responses for single-layer depositions	Variable input parameters: Arc Voltage of both wires: 12-35V, Wire Diameter: 0.8-1.2mm; Wire Feed rate in current: 30-400A, traverse speed: 40-300 (mm/min), Flow rate of shielding gas: 0-25 (NI/min); Stand-off distance (SOD): 1-7 mm Response: Visual examination for continuous deposition	Variable input parameters: Arc Voltage for NiTi: 12,14 V; Arc Voltage for Cu: 12,14 V, Traverse Speed: 120,150,180(mm/min) Constant Input parameters: Wire Diameter: 1.2mm, Wire Feed rate for NiTi in current: 300A, Wire Feed rate for Cu in current: 40A, Flow rate of shielding gas: 20 (NI/min); Stand-off distance (SOD): 3 mm Responses: Visual examination for continuous deposition, Measurement of aspect ratio
Input parameters for multi-layer depositions of NiTi20Cu SMA: Main experiments identified optimum values of voltage for NiTi is 14V, Voltage for Cu is 14V and traverse speed 150 mm/min for deposition head travel speed. This parametric combination was used to manufacture a 70 mm long multi-layer deposition from the wires of NiTi and Cu on MS base plate.		
Responses and characterization of multi-layer deposition	Analysis of microstructure and evolution of phases, chemical composition, phase transformation temperature	Mechanical characteristics: Microhardness, Tensile properties
RO-3: Comparative study of NiTi, NiTi5Cu, and NiTi20Cu using their characterizations		

Chapter 3

Details of Experimentation

This chapter presents description of different aspects related to the experiments performed for manufacturing single-layer and multi-layer depositions of NiTi_xCu SMAs by micro-plasma arc metal additive manufacturing (μ -PAMAM) process on Ti-6Al-4V substrate plate and by twin wire arc additive manufacturing (T-WAAM) process on mild steel substrate plate. It also describes measurement of different responses used for assessment of single-layer and multi-layer depositions of NiTi_xCu SMAs fabricated by μ -PAMAM and T-WAAM processes.

3.1 Deposition of NiTi_xCu SMAs by μ -PAMAM Process

This section describes preparation of powders of NiTi, NiTi₅Cu and NiTi₂₀Cu SMAs, machine for μ -PAMAM process, pilot and main experiments used to manufacture single-layer depositions of NiTi₅Cu SMA, and multi-layer depositions of NiTi, NiTi₅Cu and NiTi₂₀Cu SMAs by μ -PAMAM process.

3.1.1 Materials for μ -PAMAM Process

Powders of nickel, titanium and copper (procured from *Loba Chemie Pvt Ltd, Mumbai*) were used to prepare feedstock materials for NiTi, NiTi₅Cu and NiTi₂₀Cu SMAs. These powders had 99.5% purity and particle size in a range from 20 to 150 μ m. Powders of Ni, Ti, Cu, taken according to their at.% mentioned in Table 1, were mixed in a planetary ball milling machine (*Pulverisette 6 from Fritsch, Germany*). The mixing was carried out for 3 hours at 300 rpm using tungsten carbide balls of 6 mm diameter and maintaining ball to powder ratio as 2:1. The prepared powders of NiTi_xCu SMAs were de-moisturized for 2 hours in an oven at 80°C and then were vacuum sealed before their depositions by μ -PAMAM process. Morphology of the prepared powder for NiTi₂₀Cu is shown in Fig. 3.1.

Table 3.1: Chemical composition of the prepared powders of NiTi_xCu SMA for their depositions by μ -PAMAM process.

Alloy type	At.% of constituents			Wt.% of constituents		
	Ni	Ti	Cu	Ni	Ti	Cu
NiTi	50	50	0	55.10	44.9	0
NiTi ₅ Cu	47.5	47.5	5	51.8	42.3	5.9
NiTi ₂₀ Cu	40	40	20	42.42	34.6	22.97

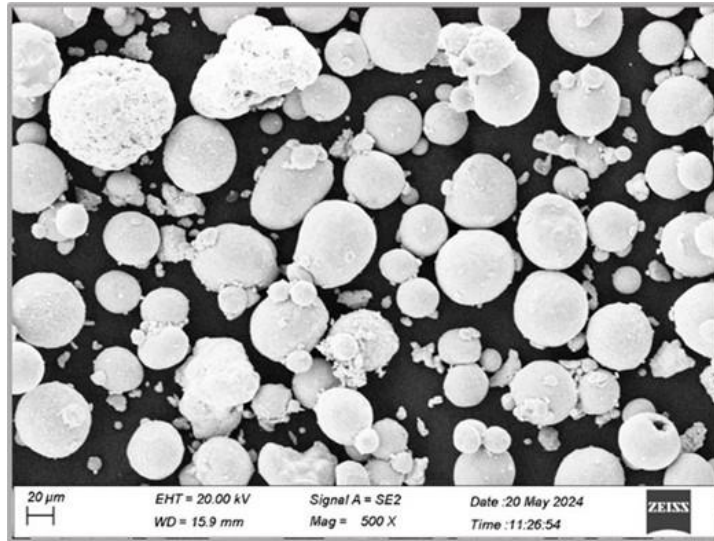


Fig. 3.1: Morphology of particles of the prepared powder of NiTi₂₀Cu SMA.

3.1.2 Machine for μ -PAMAM Process

Fig. 3.2 shows working principle of μ -PAMAM process. In this process, a direct current (DC) power supply of 440 watts is used to provide a low DC current, ranging from 0.1 to 20A, to ionize the plasma-forming gas, generating a μ -plasma arc within the nozzle and between a non-consumable tungsten electrode and the base plate. This μ -plasma arc serves as the heat source to melt the incoming feedstock material, fusing it with the base plate or the previously deposited layer. The arc is directed through a fine hole in the nozzle which ensures μ -plasma arc stability even at low currents, provides higher energy density, reduces heat-affected zone and thermal distortions and dilution. The μ -PAMAM process employs a coaxially fed inert gas, such as argon, to shield the molten feedstock material from the surrounding environment. With the electrode housed inside the nozzle, the feedstock material does not come into contact with it, allowing the process to utilize deposition materials in powder form, wire form, or a combination of both.

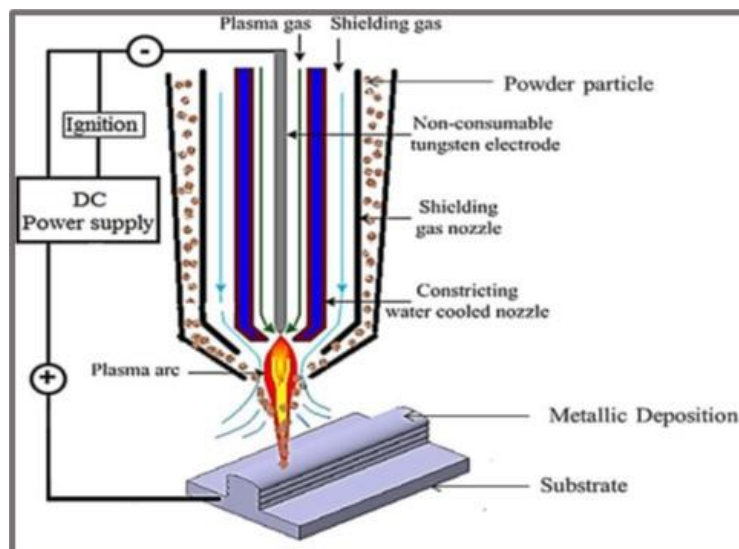


Fig. 3.2: Working principle of μ -PAMAM process.

Fig. 3.3 depicts photograph of the in-house developed 5-axis computer numerical controlled (CNC) machine for the μ -PAAM process. This machine integrates the following five key subsystems: (i) 5-axis CNC worktable that mounts the substrate plate, with its controller programmed in G and M codes via a dedicated computer, (ii) DC power supply of 440 W capacity and the cooling unit (model: *Dual Arc 82* from *Elderfield & Hall Inc., USA*). It is capable of operating in either continuous or pulsed mode and provides up to 20 A current with 0.1 A increments for μ -plasma arc generation, (iii) Feedstock material powder feeding system that supplies feedstock to the deposition head at the required flow rate. It comprises of a hopper, powder feeder, and a DC power unit for the feeding system, (iv) Plasma-forming gas and shielding gas supply system to provide argon gas for forming μ -plasma arc within the nozzle and for shielding the molten pool from atmospheric contamination, and (v) An indigenously developed deposition head featuring a μ -plasma torch at its center and four nozzles inclined at 60° to the vertical axis and positioned circumferentially at equal intervals (as shown in the enlarged view in Figure 3.3) through which feedstock material powder is delivered to it for its deposition.

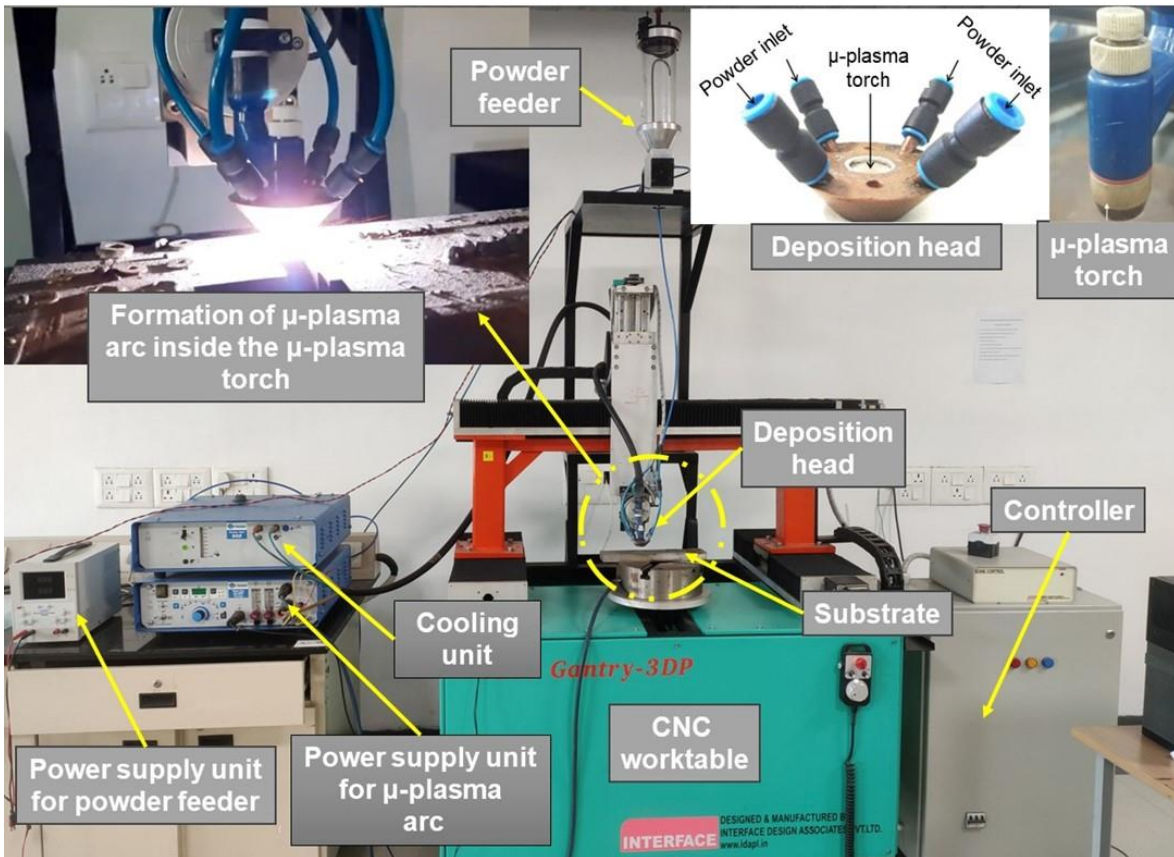


Fig. 3.3: Photograph of 5-axis CNC machine developed for μ -plasma metal additive manufacturing (μ -PAMAM) process (Arya et al., 2024).

3.1.3 Pilot and Main Experiment for μ -PAMAM Process

Experiments were designed and conducted in two different phases namely pilot experiments and main experiments. Table 3.2 presents ranges and values of μ -PAAM process parameters, and design of experiments approach used in the pilot and main experiments.

Table 3.2: Values of μ -PAMAM process parameters used in different phases of experiments.

Parameter	Range used in the pilot experiments	Values identified for the main experiments	Values identified for multi-layer depositions
Number of experiments	30	9	3
Design of experiment approach	One-factor-at-a-time	Full factorial	None
μ-PAAM process parameters for NiTi_xCu SMAs			
μ -plasma power (W)	110-440	363; 374; 385	374
Mass flow rate of feedstock material powder (g/min)	0.6-5.0	2.9	2.9
Deposition head travel speed (mm/min)	40-200	47; 51; 55	51
Flow rate of μ -plasma forming gas (Normal liter/min or NI/min)	0.1-0.5	0.25	0.25
Flow rate of shielding gas (NI/min)	3-8	4.5	4.5
Stand-off distance (mm)	5-12	8	8

Thirty pilot experiments were conducted by manufacturing single-layer depositions of NiTi₅Cu powder on Ti6Al4V alloy substrate plate having 160; 120; and 30 mm as length, width and thickness respectively. The objective was to identify optimum value/ranges of six important parameters of μ -PAMAM process for the main experiments using criterion of continuous deposition (determined through visual examination) by varying them in their following ranges: (a) μ -plasma power: 110-440 W; (b) mass flow rate of feedstock material powder: 0.6-5.0 (g/min); (c) deposition head travel speed: 40-200 (mm/min); (d) flow rate of μ -plasma forming gas 0.1- 0.5 Normal liter per minute (NI/min); (e) flowing rate of shielding gas: 3-8 (NI/min); and (f) stand of distance (SOD): 3-15 mm. The pilot experiments were conducted using one-factor-at-a-time experimental design approach in which one parameter was varied in its considered range and other parameters were kept constant at minimum values of their respective ranges. It was found that 0.25 NI/min is the minimum required flow rate of μ -plasma forming gas to produce μ -plasma arc and transmit it to the base plate. Its higher values cause melt pool to expand leaving a dimple-like imprint on the top surface of deposition. It was observed that 8 mm of SOD was adequate to assure supply of powdered material to center of the melt pool. It was found that minimum μ -plasma power 363 W was required to melt NiTi₅Cu powder hence 363; 374; 385 W were chosen as values for the main experiments. Mass flow rate of feedstock material powder more than 2 g/min allowed smooth

powder feeding and continuous deposition of NiTi5Cu powder but its value greater than 4 g/min resulted in non-uniform and partially melted deposition. Therefore, 2.9 g/min was selected for main experiment. Discontinuous deposition was formed when deposition head travel speed exceeded 55 mm/min whereas its value less than 45 mm/min resulted in a larger heat affected zone. Consequently, 47, 51, 55 mm/min were chosen for the main experiment. Summarily, the pilot experiment identifies 0.25 NI/min as flow rate of μ -plasma forming gas; 4.5 NI/min as flow rate of shielding gas; and 8 mm as SOD as their identified optimum values, and 363, 374, 385 W for μ -plasma power, 2.9 g/min for feedstock material power mass flow rate, and 47, 51, 55 mm/min for deposition head travel speed as their identified optimum ranges for conducting the main experiments. Nine main experiments were conducted by manufacturing single-layer depositions (each having 40 mm length) of NiTi5Cu alloy powder on Ti6Al4V alloy substrate plate to identify the optimum values of μ -plasma power, feedstock material powder mass flow rate, and deposition head travel speed using criteria of good quality continuous deposition having combination of minimum aspect ratio and dilution.

3.1.4 Multi-layer Deposition of NiTi_xCu SMAs by μ -PAMAM

The main experiments identified combination of 374 W for μ -plasma power and 51 mm/min for deposition head travel speed as the optimum parametric combination. It was used to manufacture multi-layer deposition of NiTi0Cu, NiTi5Cu and NiTi20Cu SMAs on Ti6Al4V substrate plate by μ -PAAM process. Each deposition was of 50 mm long and consisted of 8 depositions layers. They are referred to as the optimized depositions in the subsequent text. Aspect ratio and % dilution was studied for single-layer deposition samples. Porosity, microstructure, evolution of phases, tensile properties, microhardness, and phase transformation behaviour were studied for the samples from the optimized multi-layer depositions of NiTi0Cu, NiTi5Cu, and NiTi20Cu alloys.

3.2 Deposition of NiTi20Cu SMA by T-WAAM Process

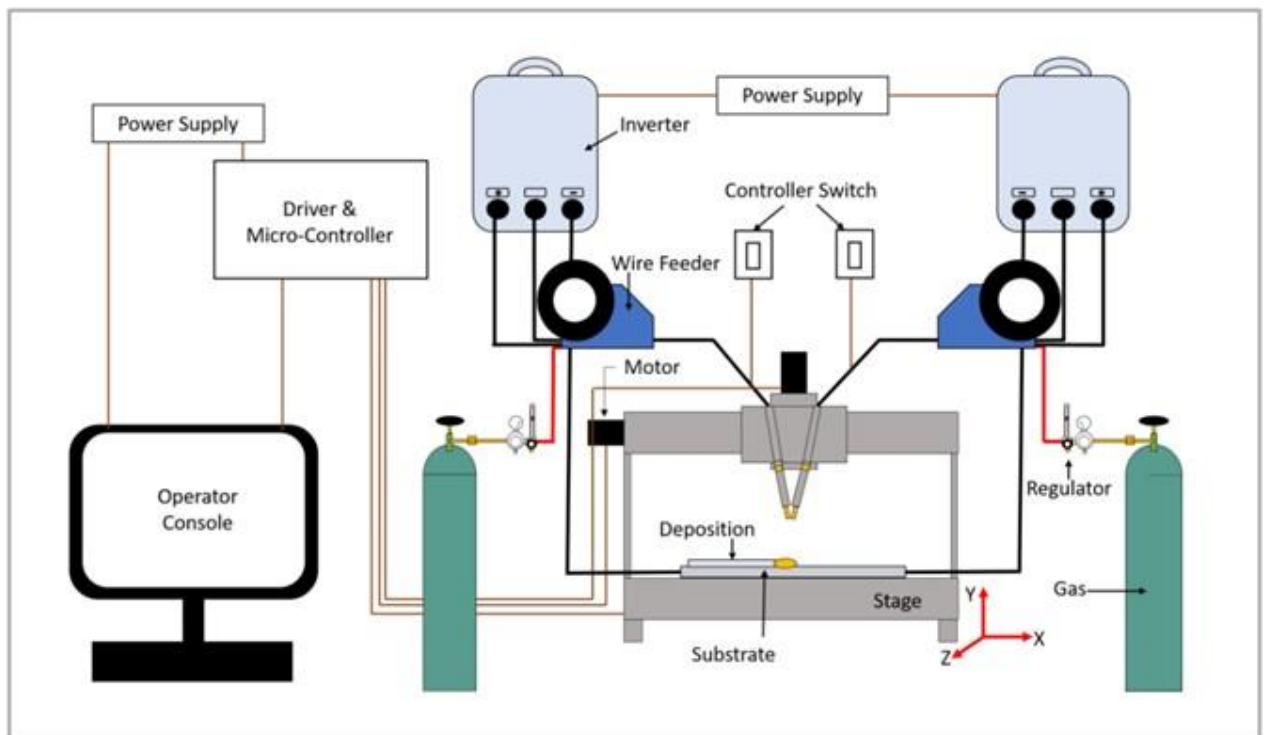
This section provides details of wires of NiTi and Cu, machine for T-WAAM process, pilot and main experiments used to manufacture single-layer and multi-layer depositions of NiTi20Cu SMA by T-WAAM process.

3.2.1 Materials for T-WAAM Process

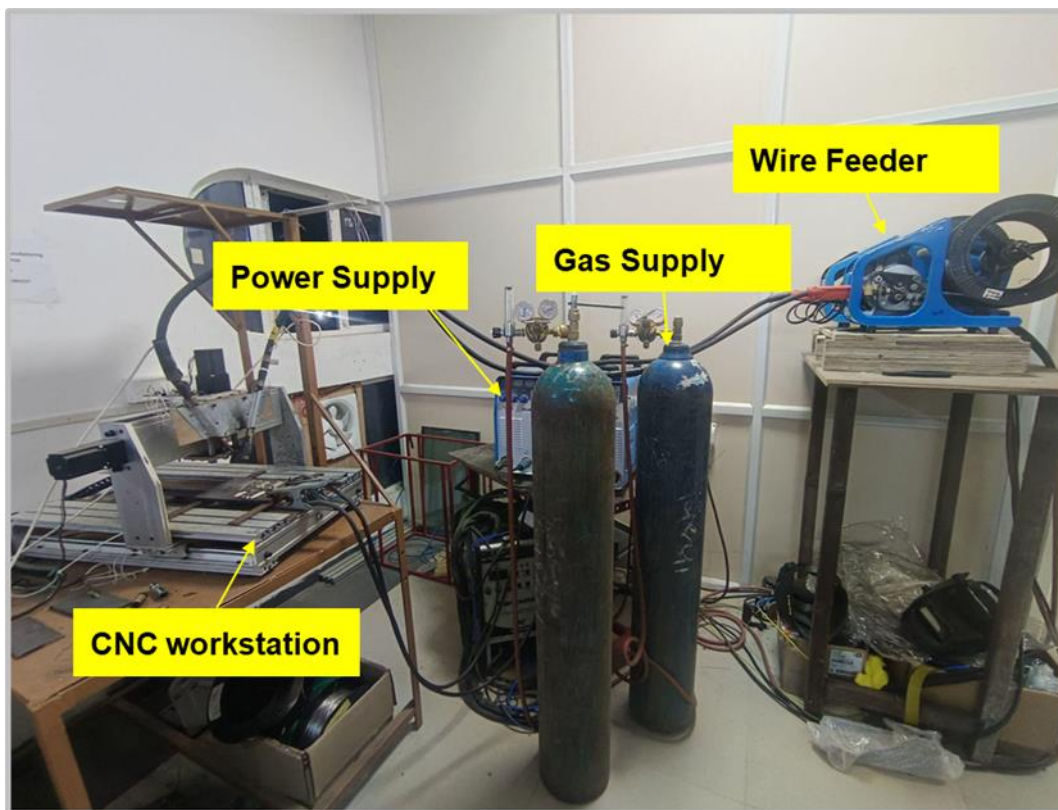
Wire of NiTi (comprising of 50 at.% of Ni and Ti) and copper wire, each having 1.2 mm diameter and purity of 99.6% (procured from *Special Materials, Mumbai*) were used as a feedstock materials for single-layer and multi-layer depositions of NiTi20Cu SMA on MS substrate plate (having 300 mm; 200 mm; and 15 mm as its length, width, and thickness respectively) by the T-WAAM process.

3.2.2 Machine for T-WAAM Process

Fig 3.4 shows schematic diagram (Fig. 3.4a) and photograph (Fig. 3.4b) of in-house developed 3-axis CNC machine for T-WAAM process which was used for single-layer and multi-layer depositions of NiTi20Cu SMA on the mild steel substrate plate. The efficiency of the machine can reach up to 85%. And it saves 30% energy as compared to the traditional machines. It has the following five units: (i) 3-axis CNC worktable to supports the substrate plate. Its controller is programmed in G and M codes via a dedicated computer, (ii) Gas metal arc-based heat source (*Make and Model: Reliable MIG 400HD*). A rectifier supplies it DC current and voltage in a range of 20 to 400 A and from 12 to 34 V respectively by converting from the 50 Hz AC power supply, (iii) Wire feeding system (*Model: CS.401Y*) to supply wires of the feedstock materials, and (iv) Two nozzles (having 60° angle between) for coaxial supply wires of feedstock materials and shielding gas (i.e., argon) to protect the melt pool from the atmospheric contamination. These nozzles are positioned at angle of 60° relative to the substrate surface. In the T-WAAM process, the supplied DC voltage creates an arc between feedstock materials and the substrate. This arc acts as a heat source to melt the incoming feedstock material and fuses it with the substrate plate or the previously deposited layer. Coaxial supply of feedstock materials and shielding gas allows maximum deposition of the materials on the substrate plate or previously deposited layers.



(a)



(b)

Fig. 3.4: Machine for T-WAAM process: (a) schematic diagram, and (b) photograph.

3.2.3 Pilot and Main Experiment for T-WAAM Process

Experiments were designed and conducted in two different phases namely pilot experiments and main experiments. Table 3.3 presents the ranges of T-WAAM process parameters used in the pilot experiments and their identified values used in the main experiments and multi-layer deposition.

Table 3.3: Values of T-WAAM process parameters used in different phases of experiments.

	Ranges used in the pilot experiments	Values identified for the main experiments	Values identified for multi-layer deposition
Number of experiments	30	12	1
Design of experiment approach	One-factor-at-a-time	Full factorial	None
T-WAAM process parameters for NiTi20Cu SMA			
Voltage for NiTi (volts)	12-35	12;14	14
Voltage for Cu (volts)	12-35	12;14	14
Deposition head traverse speed (mm/min)	40-300	120; 150; 180	150
Current for NiTi wire (A)	30-400	300	300
Current for Cu wire (A)	30-400	40	40
Flow rate of shielding gas (NI/min)	0-25	20	20
Stand-off distance (mm)	1-7	3	3

Thirty pilot experiments were conducted by manufacturing single-layer depositions of NiTi20Cu. The objective of pilot experiments was to identify optimum value/ranges of 5 important parameters of T-WAAM process for the main experiments using criterion of continuous deposition (determined through visual examination) by varying them in their following ranges: (a) Voltage range: 12 to 35 (b) Wire feed rate: 30-400(A); (c) deposition head traverse speed: 40-300 (mm/min); (d) flowing rate of shielding gas: 0-25 (NI/min); and (f) stand of distance (SOD): 1-7 mm. Pilot experiments were conducted using *one-factor-at-a-time* experimental design approach in which one parameter was varied in its considered range and other parameters were kept constant at minimum values of their respective ranges. It was observed that 3 mm of SOD was adequate to assure supply of material to center of the melt pool. It was found that minimum voltage of 12 Volts was required to melt wires of NiTi and Cu each therefore 12 Volts and 14 Volts were identified as voltage values for feeding the wires of both NiTi and Cu for the main experiments. Current supply (an indirect measure of mass flow rate of feedstock wire) more than 30A allowed smooth feeding and continuous deposition and its value greater than 400A resulted in non-uniform and partially melted deposition. Therefore, current values of 300A for NiTi and 40A for Cu were selected for the main experiment. Discontinuous deposition was formed when deposition head traverse speed exceeded 180 mm/min whereas its value less than 120 mm/min resulted in a larger heat affected zone. Consequently, deposition head traverse speed values of 120,150,180 mm/min were chosen for the main experiment. Twelve full factorial main experiments were conducted by manufacturing single-layer depositions (each having 50 mm deposition length) of NiTi20Cu on the MS substrate plate. The objective was to identify optimum parametric combination of deposition head traverse speed, and voltage values for feedstock wire of NiTi and Cu using the criteria of good quality continuous deposition with minimum aspect ratio.

3.2.4 Multilayer Deposition of NiTi20Cu by T-WAAM Process

The main experiments identified the combination of 150 mm/min as deposition head traverse speed and 14 Volts as voltage for feeding the wires of both NiTi and Cu as the optimum parametric combination. It was used to manufacture 70 mm long multi-layer deposition (consisting of 12 deposition layers) of NiTi20Cu alloy on MS substrate plate by T-WAAM process. It is referred to as the optimized deposition in the subsequent text. Aspect ratio was studied for the single-layer deposition samples. Microstructure, evolution of phases, and microhardness, tensile properties, phase transformation effect were studied for the sample of optimized multi-layer deposition of NiTi20Cu SMA.

3.3 Measurement of the Responses

Fig. 3.5 presents photograph of the optimized multi-layer deposition showing locations of the different samples cut along its build direction for evaluation of microstructure, evolution of phases, microhardness, tensile properties, and phase transformation behavior of NiTi_xCu SMAs developed by μ -PAMAM and T-WAAM processes.

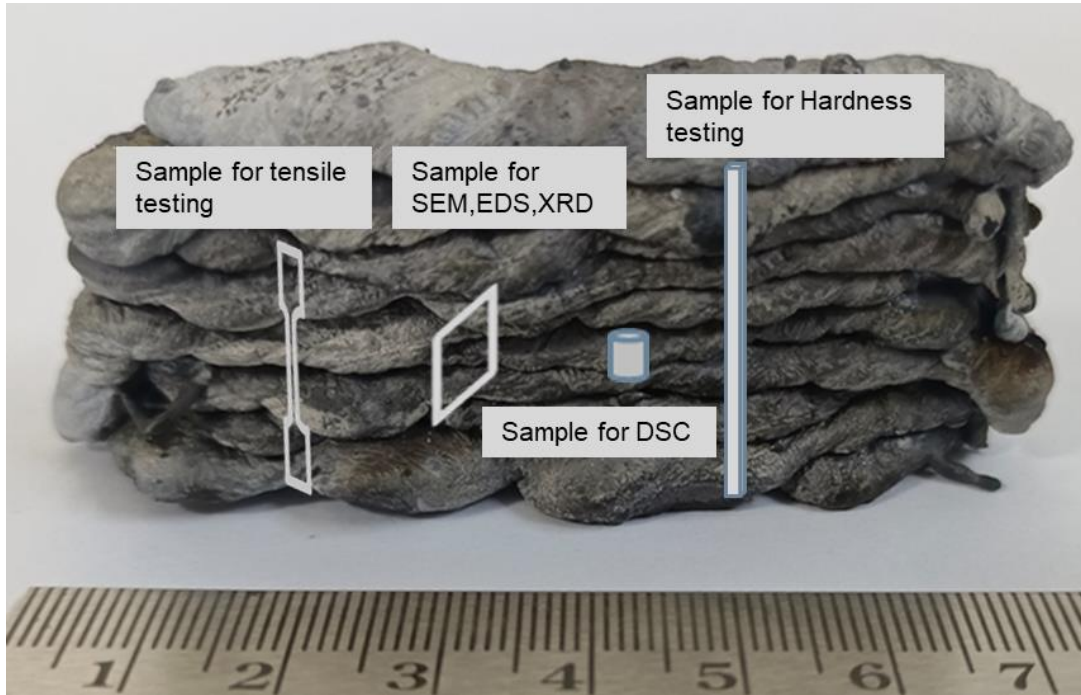


Fig. 3.5: Location of different samples from the optimized multi-layer deposition along its the build direction for evaluation of different responses.

3.3.1 Aspect Ratio and Dilution

Nine samples and 12 samples from the centre of each single-layer deposition of NiTi₅Cu manufactured by the μ -PAMAM and T-WAAM process respectively, were cut by wire spark erosion machining (WSEM) process (*Ecocut* model from *Electronica India Ltd. Pune, India*). Each cut sample was cold mounted in a polymeric resin with the help of liquid binder and polished up to 2000 grit size silicon carbide emery papers. Stereo microscope (*Leica EZA HD* from *Leica, Germany*) was used to compute its deposition width ' W ' (mm) and deposition height ' H ' (mm), and its aspect ratio ' AR ' was computed as the ratio of its ' W ' to ' H ' as shown in Fig. 3.6. The deposition area ' Q ' and dilution area ' P ' for the μ -PAMAM manufactured single-layer deposition sample were measured by importing its stereo-microscopic image to the *ImageJ* software. Dilution ' D ' is a measure of the amount of the deposited material mixed with the substrate material. It is the ratio of dilution area ' P ' to the summation of dilution area ' P ' and deposition area ' Q ' as depicted in Fig. 3.6. It is an

important parameter whose higher values (i.e., more than 10%) are unfavourable since it reduces deposition quality while increasing thermal distortion and residual stresses.

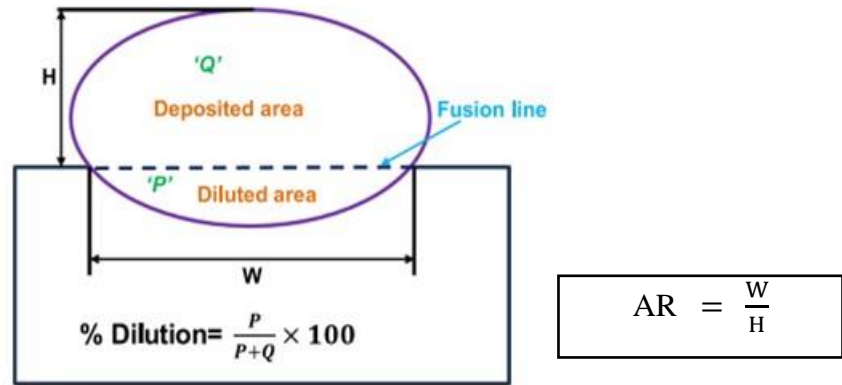


Fig. 3.6: Schematic view of single-layer deposition (where, ' W ' is deposition width; ' H ' is deposition height; ' AR ' is aspect ratio; ' D ' is dilution; ' P ' is diluted area; ' Q ' is deposition area).

3.3.2 Microstructure and Chemical Composition

One sample from each optimized multi-layer deposition of NiTi, NiTi5Cu, and NiTi20Cu manufactured by μ -PAMAM process and NiTi20Cu manufactured by T-WAMM process, was cut transversely (as per the location shown in Fig. 3.5) by the WSEM process) to study its microstructure, chemical composition, elemental mapping and formation of phases. Each cut sample was cold mounted in a polymeric resin with the help of liquid binder and polished up to 2500 grade using silicon carbide emery paper followed by cloth polishing with the help of diamond pastes with the fineness of 2.5 μm and 1 μm . The polished sample was dipped in the freshly prepared etchant solution consisting of 10 ml HF, 40 ml HNO₃ and 50 ml H₂O for 15 seconds and then rinsed in running water. Microstructure of each prepared sample was obtained by field-emission SEM (*supra 25* from *carl Zeiss*). Chemical composition of a prepared sample was determined using its energy dispersive spectroscopy (EDX) facility.

3.3.3 Evolution of Phases

Evolution of phases in an optimized deposition sample was analysed by x-ray diffraction (XRD) (*D₂-Phaser* from *Bruker, USA*) using 40 kV voltage, 30 mA current, 2θ range of 20-100° with 0.02 step size, 1 second dwell time, and Cu-K α radiation ($\lambda = 1.5418 \text{ \AA}$). Different phases present in an optimized multi-layer deposition sample and their crystal structures were identified by matching the characteristic peaks present in its XRD with the Joint Committee on Powder Diffraction Standards (JCPDS) database.

3.3.4 Tensile Testing

Two samples were cut by the WSEM process from each optimized multi-layer deposition (as per the location shown in Fig. 3.6) of NiTi, NiTi5Cu, and NiTi20Cu manufactured by μ -PAMAM process and NiTi20Cu manufactured by T-WAMM process. Each sample, cut

following the ASTM-E8 standard, has a length of 10 mm; 4.5 mm gauge length; 1 mm gauge width; and 1 mm thickness to ensure same elongation before failure in the tensile testing. Tensile testing was carried out on the universal tensile testing machine (*Model: AGX-V series, make: Shimadzu, Japan*) at room temperature using an elongation rate of 1 mm/min to evaluate ultimate tensile strength and strain of each prepared sample.

3.3.5 Microhardness Evaluation

One sample from was cut by the WSEM process along the build direction (i.e., along the deposition height) of each optimized multi-layer deposition (as per the location shown in Fig. 3.6) of NiTi, NiTi5Cu, and NiTi20Cu manufactured by μ -PAMAM process and NiTi20Cu manufactured by T-WAMM process. Each cut sample was cold mounted in a polymeric resin with the help of liquid binder and polished up to 2500 grade using silicon carbide emery paper. Vicker's microhardness of each sample was measured on the microhardness measuring equipment (*VMH 002V from Walter UHL Germany*) applying 200 g load for 15 seconds duration as per ASTM E92-82 standard. Twenty measurements of microhardness were taken for each sample at different locations along its build direction at an interval of 1 mm to obtain its microhardness profile.

3.3.6 Transformation of Phases

One cuboidal sample was cut transversely (as per the location shown in Fig. 3.6) by WSEM process from each optimized multi-layer deposition of NiTi, NiTi5Cu, and NiTi20Cu manufactured by μ -PAMAM process and NiTi20Cu manufactured by T-WAMM process to study its phase transformation behaviour. Weight of each sample was kept between 20-40 gm. The phase transformation behaviour was studied through the differential scanning calorimetry (DSC) equipment (*Model- I PerkinElmer DSC 8000*) using the measurement temperature in a range from -50 to 150 °C and heating and cooling rate as 10°C/ min.

This chapter presented description of preparation of powders to develop NiTi_xCu by μ -PAMAM process by mixing 5at.% and 20at.% of Cu with powders of Ni and Ti, machines for μ -PAMAM and T-WAAM process, details of experimentations by μ -PAMAM and T-WAAM process, preparation of samples and procedure for evaluation of aspect ratio, dilution, microstructure, evolution of phases, tensile properties, phase transformation behaviour of the developed SMAs. *Next chapter* presents the results for the single-layer deposition and optimized multi-layer depositions of NiTi_xCu SMAs and NiTi20Cu SMA fabricated by μ -PAMAM and T-WAAM process respectively, results and analysis of aspect ratio and dilution for the single-layer depositions, and analysis of microstructure, formation of phases, tensile properties, microhardness, and phase transformation behaviour for optimized multi-layer depositions.

Chapter 4

Results and Discussion

This presents the results for the single-layer depositions of NiTi, NiTi5Cu and NiTi20 Cu SMA fabricated by μ -PAMAM process during the main experiments and single-layer depositions of NiTi20Cu manufactured by T-WAAM process along with results for their optimized multi-layer depositions. It also presents results and analysis of aspect ratio and dilution for the single-layer depositions of the developed SMAs, and analysis of microstructure, formation of phases, tensile properties, microhardness, and phase transformation behaviour for optimized multi-layer depositions.

4.1 Characteristics of Single-layer Depositions

This section presents results for the nine single-layer depositions of NiTi5Cu SMA developed by μ -PAMAM process on Ti6Al4V substrate plate and for the twelve single-layer depositions of NiTi20Cu SMA manufactured by T-WAAM process on the MS substrate plate during their corresponding full factorial main experiments. The results are presented through their photographs, classification (i.e. uniform continuous deposition and non-uniform continuous), deposition characteristics (i.e., deposition height, deposition width, aspect ratio, and dilution). The objective of the single-layer deposition was to identify optimum parametric combination using the criteria of good quality uniform continuous deposition with minimum aspect ratio for fabricating the optimized multi-layer deposition of NiTi_xCu SMAs.

4.1.1 Single-layer Depositions by μ -PAMAM Process

Fig. 4.1 shows photograph of top views (obtained from the stereo-zoom microscope) of nine the single-layer depositions of NiTi5Cu SMA manufactured by the μ -PAMAM process on Ti6Al4V substrate plate. These depositions are categorized according to their quality as uniform continuous deposition (UCD) as depicted in Fig.4.1a and non-uniform continuous deposition (NCD) as shown in Fig. 4.1b. Table 4.1 presents values of their measured responses i.e., deposition height ' H ' and deposition width ' W ' and their computed responses i.e., aspect ratio ' AR ' and dilution ' D ' corresponding to the full factorial combinations of μ -plasma power and deposition head travel speed.

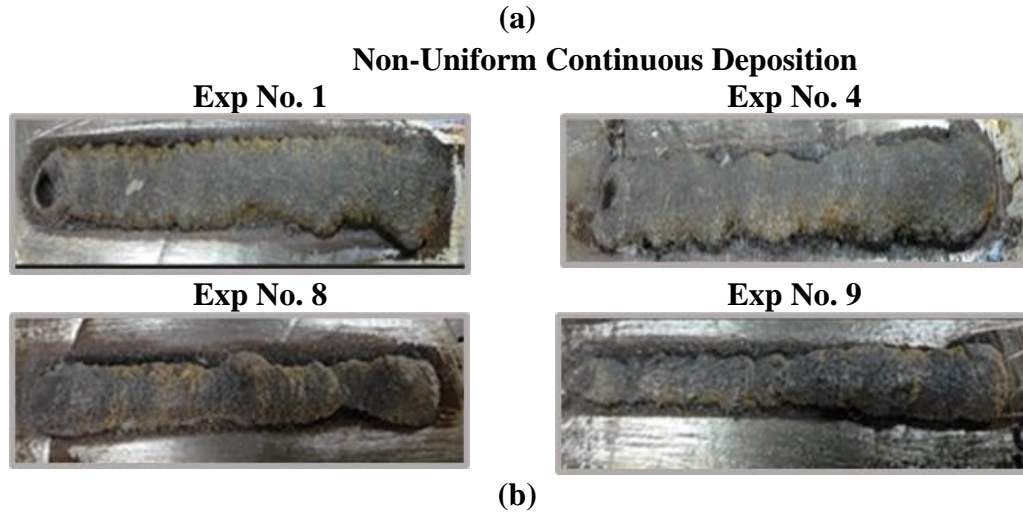
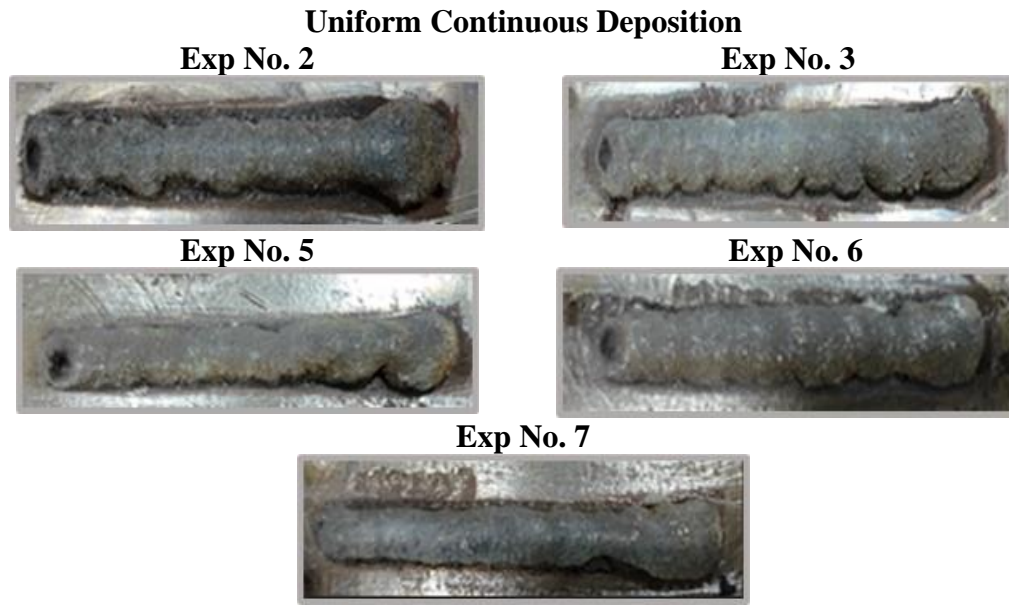


Fig. 4.1: Photographs of single-layer deposition of NiTi5Cu by μ -PAMAM process: (a) uniform continuous deposition, and (b) non-uniform continuous deposition.

Table 4.1: Measured and computed responses for single-layer deposition of NiTi5Cu SMA by μ -PAMAM process for different combinations of μ -plasma power and deposition head travel speed.

Exp. No	Measured responses		Computed responses			
	μ -plasma power (W)	Deposition head travel speed (mm/min)	Width (mm)	Height (mm)	Aspect ratio	%Dilution
Uniform Continuous Deposition						
2	363	51	5.30	3.63	1.46	10.7
3	363	55	5.05	3.23	1.56	10
5	374	51	5.55	3.63	1.53	8.3
6	374	55	5.60	3.23	1.73	10.7
7	385	47	6.09	3.77	1.61	8.95
Non-Uniform Continuous Deposition						
1	363	47	5.40	4.22	1.27	14.25
4	374	47	5.79	4.02	1.44	10
8	385	51	5.74	3.29	1.74	9.45
9	385	55	5.67	3.04	1.86	13.8

It can be observed from Fig.4.1b and Table 4.1 that four single-layer depositions corresponding to Exp. No. 1, 4, 8 and 9, have non-uniformity in their deposition width along their deposition length and they are categorized as *non-uniform continuous deposition* (NCD). They are obtained for the following combinations: (i) small or medium value of μ -plasma power and small value of deposition head travel speed (Exp. no. 1 and 4), and (ii) large value of μ -plasma power and medium or large value of deposition head travel speed (Exp. no. 8 and 9). These parametric combinations resulted in variable deposition width along the deposition length. Five single-layer depositions corresponding to Exp. no. 2, 3, 5, 6 and 7 (Fig. 4.1a) demonstrated continuity and uniformity in their deposition width along their deposition length and they are categorized as *uniform continuous deposition* (UCD). They are obtained for the following parametric combinations: (i) small value of μ -plasma power and medium or large value of deposition head travel speed (Exp. no. 2, 3), (ii) medium value of μ -plasma power and medium or large value of deposition head travel speed (Exp. no. 5, 6), and (iii) large value of μ -plasma power and small value of travel speed μ -plasma (Exp. no.7). It implies that medium value for μ -plasma power enables use of wider range of deposition head travel speed. Increase in μ -plasma power increases width and dilution of single-layer depositions of NiTi5Cu SMA but decreases its deposition height. It is due to increase in heat input to the melt pool with increase in μ -plasma power which in turn increases the dilution. It also increases the temperature inside the melt pool thus reducing its viscosity which allows more free movement of the molten material thus increasing deposition width with reduction in the deposition height. More heat input to the melt pool for a given flow rate of the feedstock material powder will increase melting of more powder, thus increasing powder deposition efficiency. Increase in deposition head travel speed decreases deposition width, deposition height, and dilution of a single-layer deposition of NiTi5Cu SMA. It is because of reduction in time available for μ -plasma to transfer heat to the melt pool, thus reducing its temperature. Smaller temperature will decrease viscosity of the molten material which obstructs its movement thus reducing deposition width but increases height of a single-layer deposition. Large value of deposition head travel speed will not allow μ -plasma to deliver sufficient heat energy to melt the feedstock material powder which reduces dilution resulting in a weaker bonding with the substrate material.

The parametric combination having μ -plasma power as 374 W and deposition head travel speed as 51 mm/min (corresponding to Exp. No. 5) which yielded UCD with minimum value of dilution, was identified as the optimum parametric combination for manufacturing optimized multi-layer depositions of NiTi, NiTi5Cu, and NiTi20Cu SMA by μ -PAMAM process on Ti6Al4V substrate plate.

4.1.2 Single-layer Deposition by T-WAAM Process

Fig 4.2 presents photographs of top views of 12 single-layer depositions of NiTi20Cu SMA manufactured by T-WAAM process on the MS substrate plate. According to their quality, they are categorized as UCD (Fig 4.2a) and NCD (Fig. 4.2b). Table 4.2 presents values of their measured responses and computed aspect ratio corresponding to full factorial combinations of voltages for wires of NiTi and Cu and deposition head traverse speed.

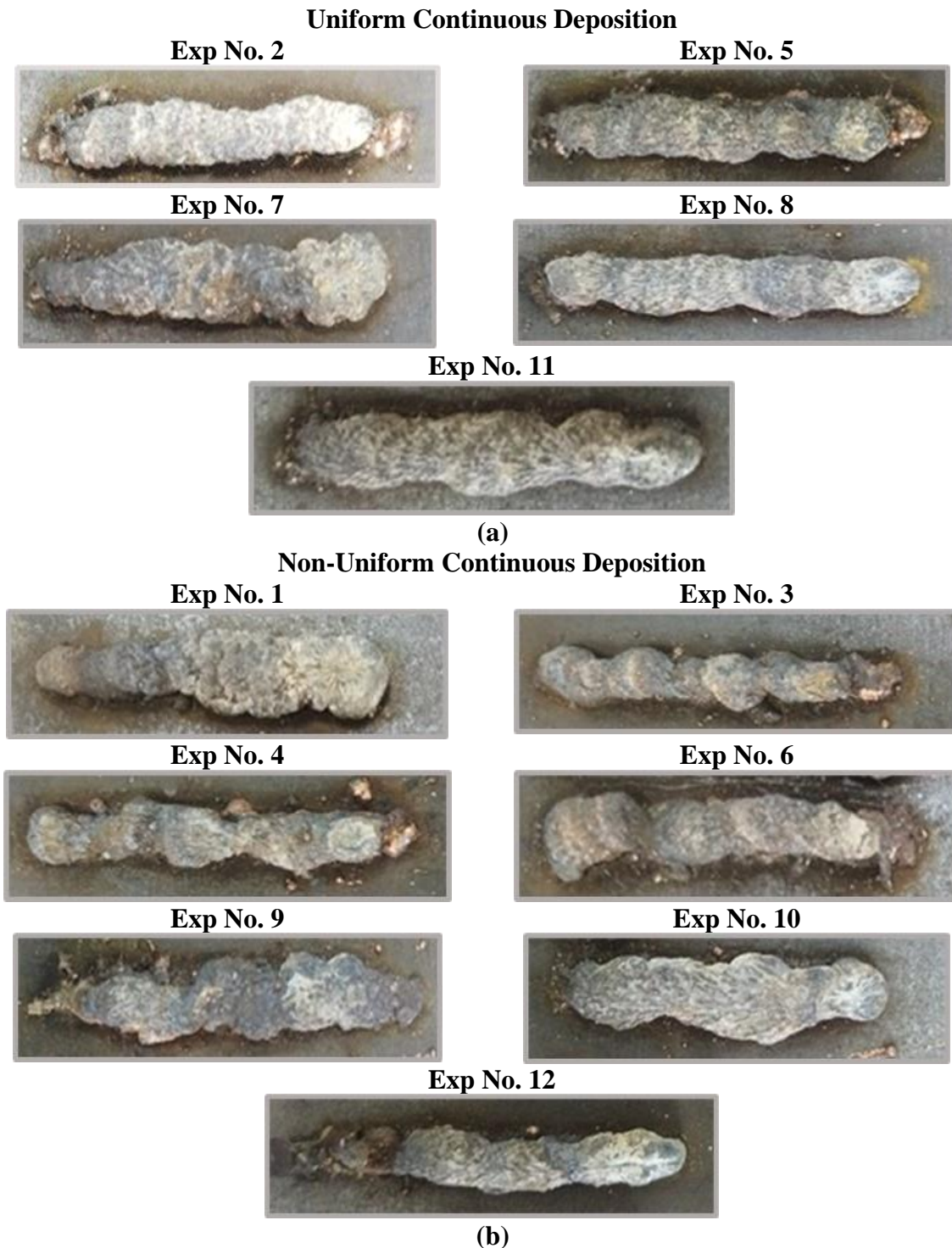


Fig. 4.2: Photographs of single-layer depositions of NiTi20Cu SMA fabricated by T-WAAM process: (a) Uniform continuous depositions, and (b) Nonuniform continuous depositions.

Table 4.2: Measured and computed responses for single-layer deposition of NiTi20Cu SMA by T-WAAM process for various combinations of voltages and deposition head travel speed.

Exp. No	Measured responses			Computed responses		
	Voltage for NiTi wire	Voltage for Cu wire	Deposition head traverse speed (mm/min)	Width (mm)	Height (mm)	Aspect ratio
Uniform Continuous Deposition						
2	12	12	150	7.801	6.393	1.220
5	14	14	150	6.029	6.076	0.992
7	12	12	120	8.973	6.361	1.41
8	12	14	150	7.057	6.076	1.16
11	14	12	150	6.978	6.061	1.151
Non-Uniform Continuous Deposition						
1	12	14	120	7.374	6.646	1.109
3	12	12	180	6.741	7.025	0.959
4	14	12	120	7.785	5.491	1.41
6	14	12	180	6.741	5.475	1.173
9	12	14	180	6.076	5.997	1.013
10	14	14	120	7.188	5.108	1.407
12	14	14	180	6.125	6.029	1.015

It can be observed from Fig 4.2 and Table 4.2 that 7 single-layer depositions corresponding to Exp. No. 1,3,4,6,9,10 and 12 have non-uniformity in their deposition width along their deposition length and they are categorized as non-uniform continuous deposition (NCD). They are obtained for following parametric combinations: (i) small value of voltage (i.e., 12 volts for the wire of both Cu and NiTi) and large value of travel speed of deposition (Exp. no. 3), and (ii) large values of voltage (i.e., 14 volts for the wire of both Cu and NiTi) and small or large value of deposition head travel speed (Exp. No. 10 and 12), and (iii) medium value of voltage (i.e., combination of 12 and 14 volts for the wire of Cu and NiTi) and small or large value of deposition head travel speed (Exp No. 1, 4, 6 and 9). These parametric combinations yielded variable deposition width along the deposition length. Five single-layer depositions corresponding to Exp. No. 2, 5, 7, 8 and 11 (Fig. 4.2a) demonstrated continuity and uniformity in their deposition width along their deposition length and they are classified as uniform continuous deposition (UCD). They are obtained for the following parametric combinations: (i) small or large values of voltage and medium value of deposition head travel speed (Exp. No. 2 and 5), (ii) medium values of voltage and deposition head travel speed (Exp. No. 8 and 11), and (iii) small values of voltage and deposition head travel speed (Exp. No. 7). Increase in wire voltage increases width of single-layer deposition of NiTi20Cu SMA but decreases its deposition height. It is due to increase in heat input to the

melt pool with increase in wire voltage. It also increases temperature inside the melt pool thus reducing its viscosity which allows more free movement of the molten material thus increasing deposition width and decreasing deposition height of a single-layer deposition. Increase in deposition head travel speed decreases deposition width and deposition height of NiTi20Cu SMA. It is because of reduction in time available for the arc to transfer heat to melt pool thus reducing its temperature which in turn reduces viscosity of the melt pool thus obstructing movement of the molten material. It reduces deposition width but increases height of a single-layer deposition.

The parametric combination having 14 Volts as the voltage value for the wires of NiTi and Cu and 150 mm/min as deposition head travel speed (corresponding to Exp. No. 5) which yielded UCD with minimum value of aspect ratio, was identified as the optimum parametric combination for manufacturing optimized multi-layer depositions of NiTi20Cu SMA by T-WAMM process on the MS substrate plate.

4.2 Optimized Multi-layer Depositions of NiTi_xCu SMAs

Optimized multi-layer deposition of NiTi0Cu, NiTi5Cu and NiTi20Cu each (consisting of 8 layers) was manufactured by the μ -PAAM process on Ti6Al4V substrate plate using the optimum parametric combination identified from the main experiments (i.e., μ -plasma power as 374 W and deposition head travel speed as 51 mm/min). Fig. 4.3 depicts their photographs. Similarly, optimized multi-layer deposition of NiTi20Cu SMA each (consisting of 12 layers) was manufactured by T-WAAM process on the MS substrate using the optimum parametric combination identified from the main experiments (i.e., 14 Volts as the voltage for the wires of NiTi and Cu and 150 mm/min as deposition head travel speed). Figure 4.4 shows its photograph.



(a)



(b)



(c)

Fig. 4.3: Optimized multi-layer deposition of NiTiCu SMA manufactured by μ -PAMAM process: (a) NiTi, (b) NiTi5Cu, and (c) NiTi20Cu.

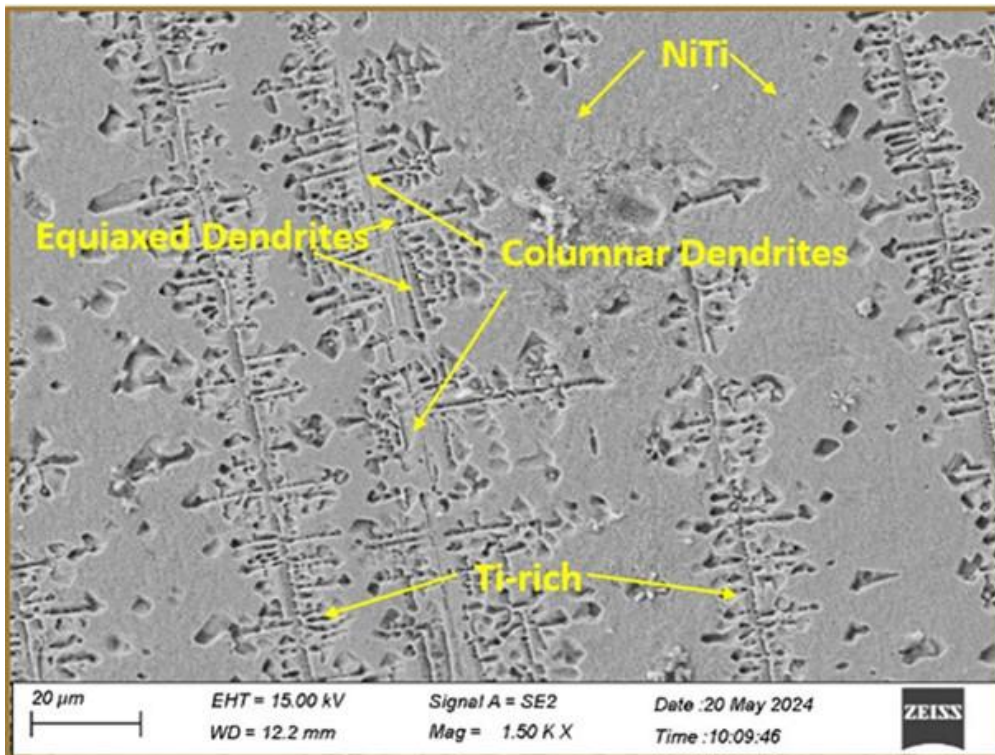


Fig. 4.4: Optimized multi-layer deposition of NiTi20Cu SMA fabricated by T-WAAM process.

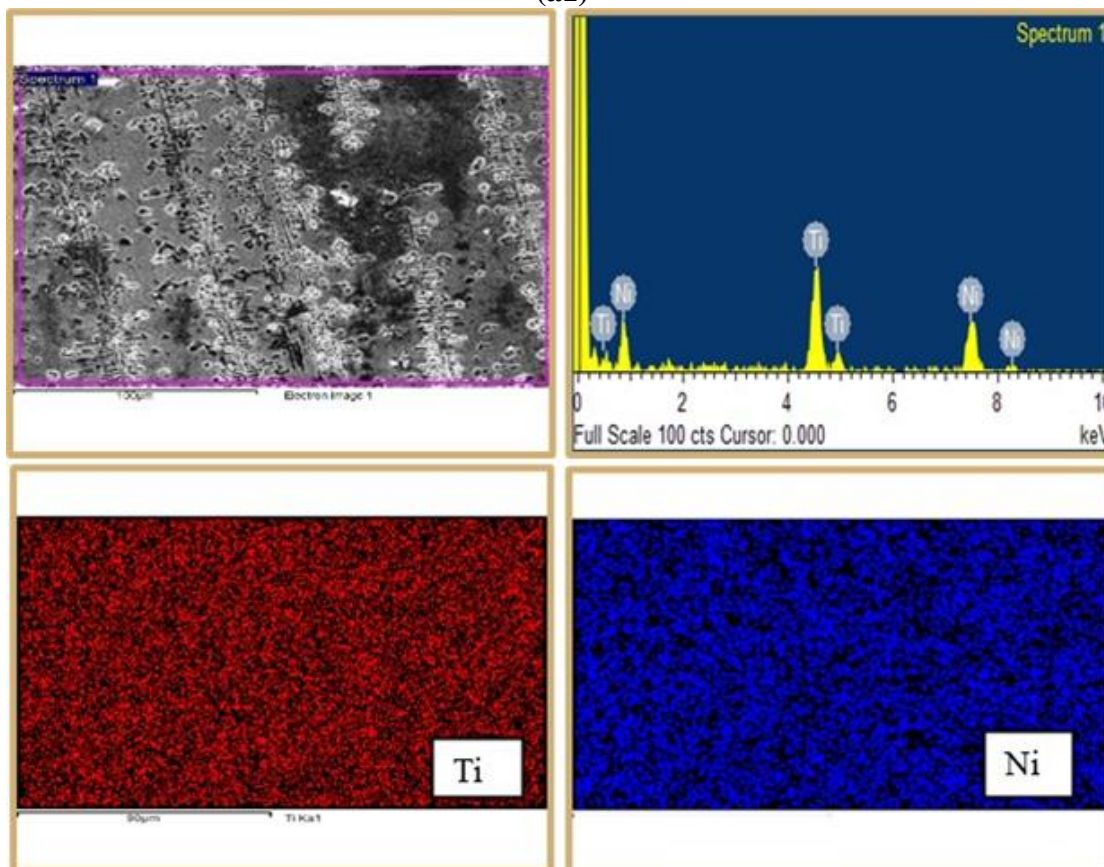
Following conclusions can be drawn from the comparison of the optimized multi-layer deposition of NiTi20Cu SMA manufactured by process (Fig. 4.3c) with that manufactured by T-WAAM process (Fig. 4.4): (i) μ -PAMAM manufactured multi-layer deposition has better surface quality and better bonding between the different layers than that manufactured by T-WAAM process. It is due to use of feedstock material in the powder form in μ -PAMAM process, (ii) T-WAAM manufactured multi-layer deposition has more oxides on its surface than that manufactured by μ -PAMAM process. It is due to use of more power and higher susceptibility towards atmospheric contamination in T-WAAM process.

4.3 Analysis of Microstructure and Chemical Composition

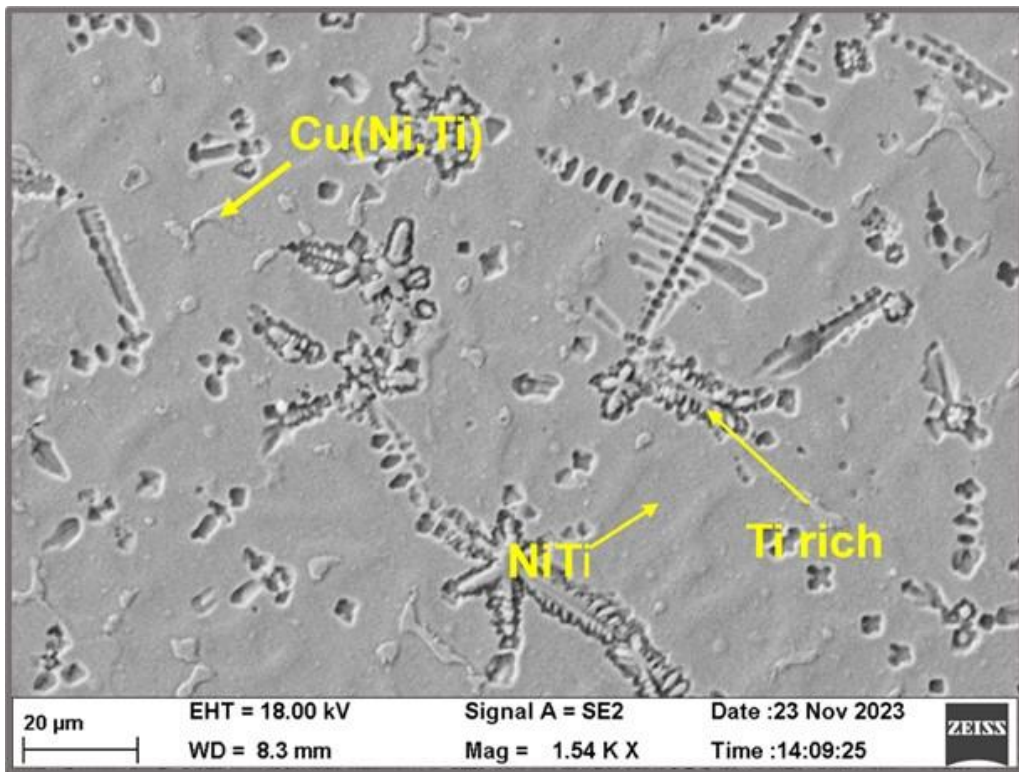
Fig 4.5 presents SEM images showing microstructure of the optimized multi-layer deposition samples of NiTi (Fig. 4.5a1), NiTi5Cu (Fig. 4.5b1) and NiTi20Cu (Fig. 4.5c1) SMA manufactured by μ -PAMAM process, and NiTi20Cu SMA manufactured by T-WAAM process (Fig. 4.5d1). Their elemental spectrum and elemental mapping images obtained by EDX are presented in Figs 4.5a2, 4.5b2, 4.5c2, and 4.5d2 respectively. Colored elemental mapping images provide a visual representation of distribution of constituents in an alloy. Table 4.3 complements this by presenting their elemental distribution (by at. %).



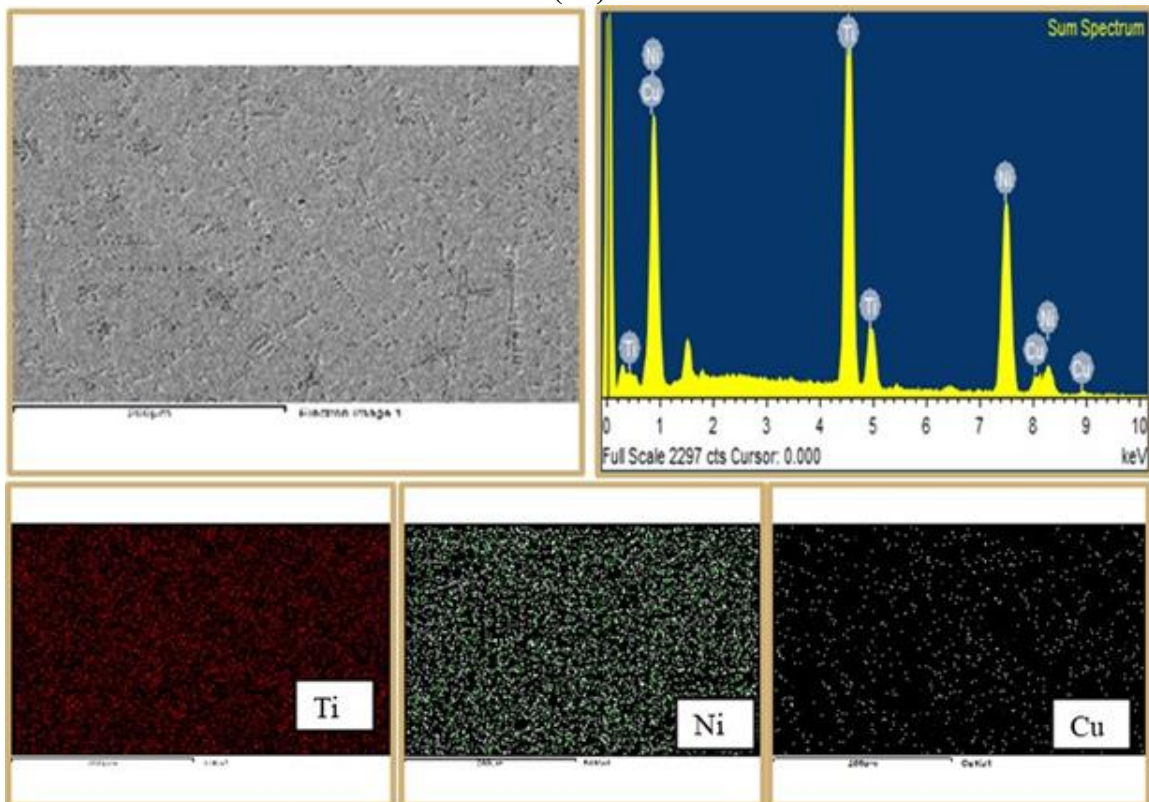
(a1)



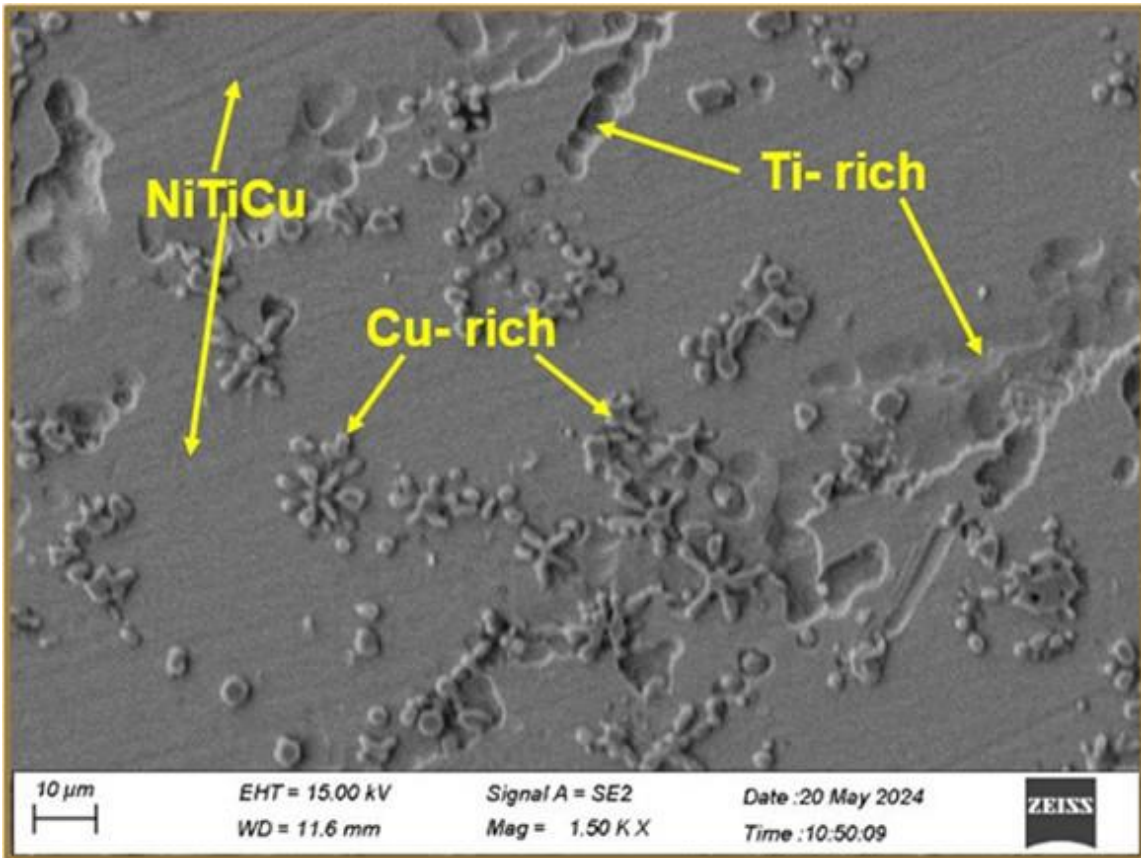
(a2)



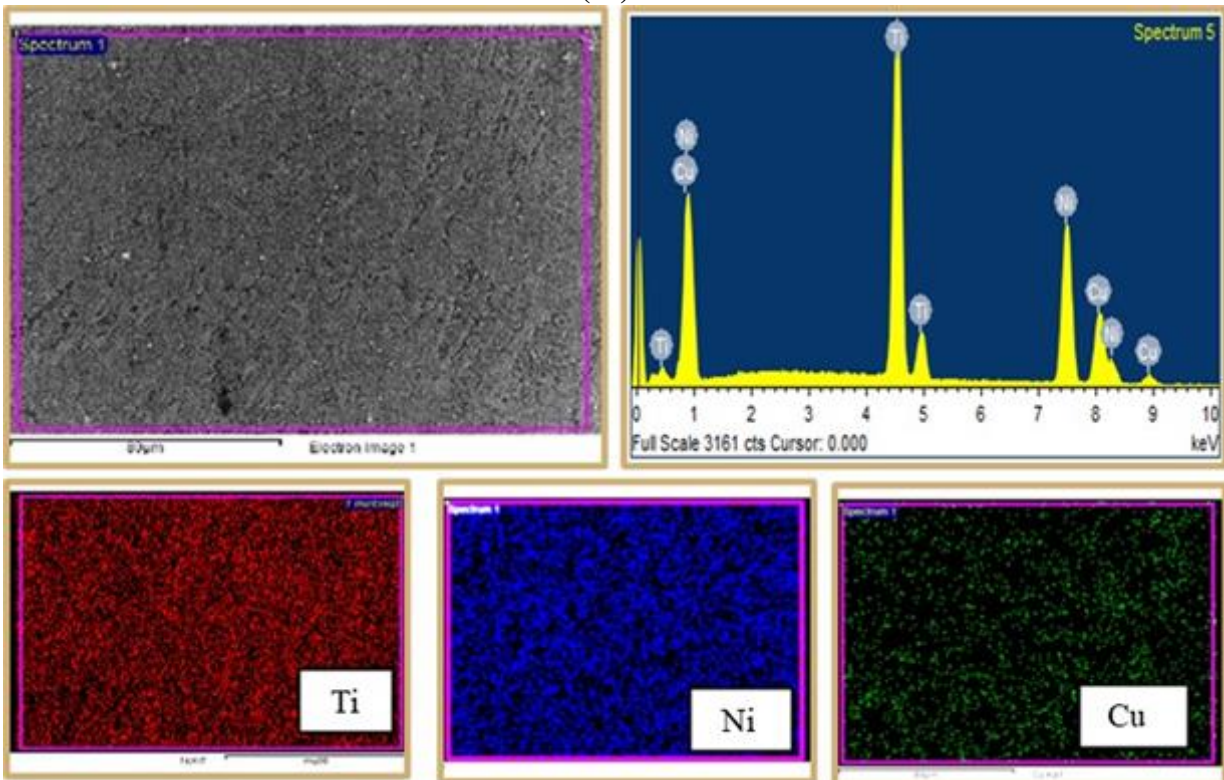
(b1)



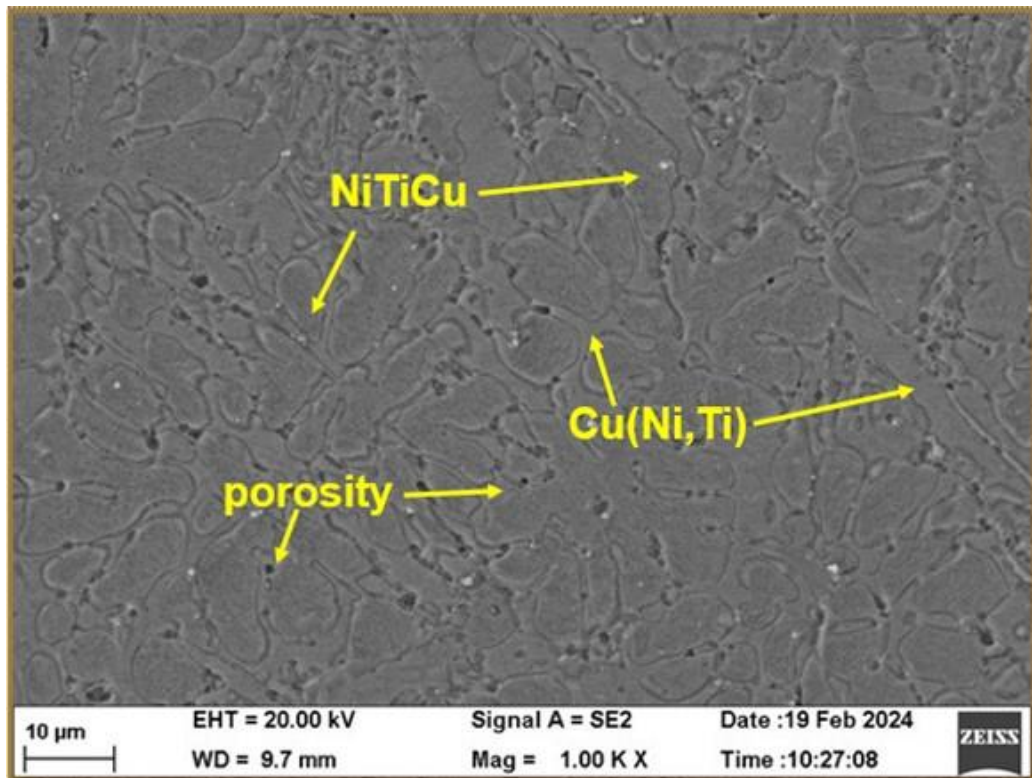
(b2)



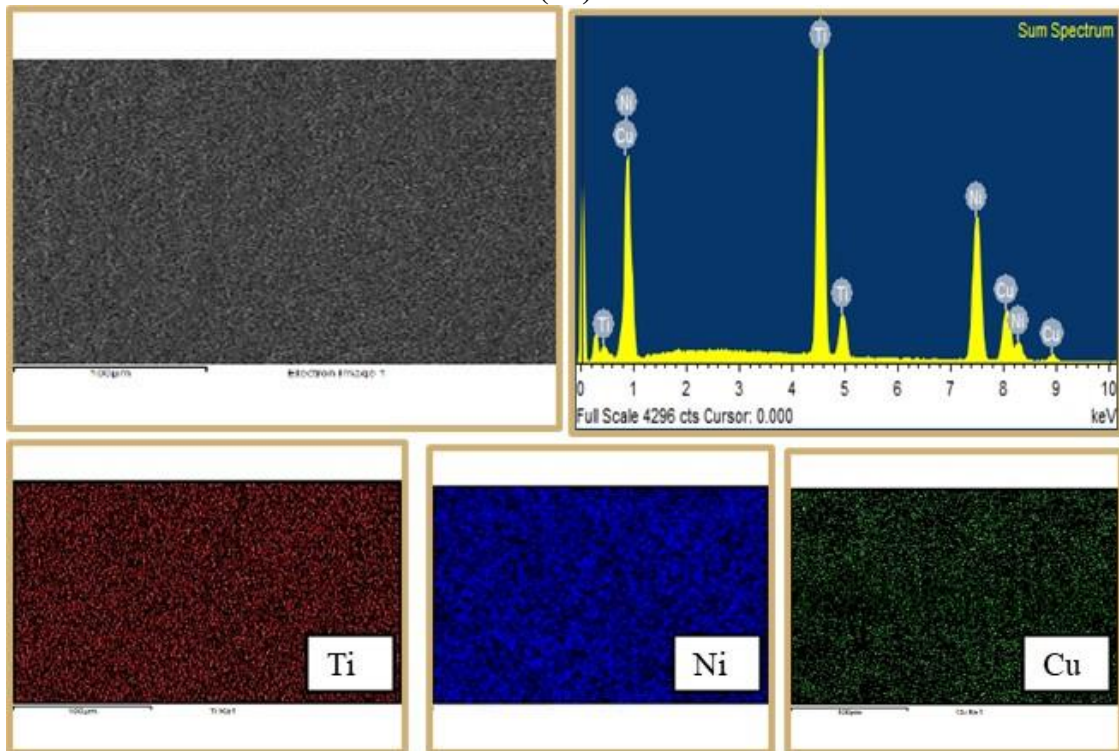
(c1)



(c2)



(d1)



(d2)

Fig. 4.5: Microstructure, elemental mapping, and chemical composition of optimized multi-layer depositions for: **(a1 and a2)** μ -PAMAM manufactured NiTi SMA, **(b1 and b2)** μ -PAMAM manufactured NiTi5Cu SMA, **(c1 and c2)** μ -PAMAM manufactured NiTi20Cu, and **(d1 and d2)** T-WAAM manufactured NiTi20Cu SMA.

Table 4.3: Elemental distribution (by at. %) in the optimized multi-layer depositions of NiTiXCu SMAs.

Alloy and process	Ti	Ni	Cu
NiTi by μ -PAMAM process	51.56	48.44	0
NiTi5Cu by μ -PAMAM process	51.37	43.26	5.37
NiTi20Cu by μ -PAMAM process	41.47	38.96	19.57
NiTi20Cu by T-WAAM process	41.01	38.82	20.17

Microstructure of the optimized multi-layer deposition of NiTi SMA developed by μ -PAMAM process (Fig. 4.5a1) primarily consists of columnar dendritic structure which is typically observed during solidification of an alloy developed by an AM process. It also shows formation of Ti-rich phase in the dendritic regions which is confirmed by its elemental spectrum (Fig. 4.5a2) and its XRD pattern (Fig. 4.6) which indicates presence of a NiTi matrix along with intermetallic phase Ti_2Ni . Microstructure of the optimized multi-layer deposition of NiTi5Cu SMA developed by μ -PAMAM process (Fig. 4.5b1) reveals it also comprises of columnar dendritic structure with formation of Ti-rich phase in it which is confirmed by its by its elemental spectrum (Fig. 4.5b2). But addition of 5 at.% copper leads to formation of Cu (Ni, Ti) phase suggesting some degree of Cu segregation and formation of Cu-containing intermetallic phase. This addition appears to alter the segregation pattern of Ni and Ti during the solidification thus potentially affecting formation of dendritic and interdendritic regions. Microstructure of the optimized multi-layer deposition of NiTi20Cu SMA by μ -PAMAM process (Fig. 4.5c1) reveals that addition of 20at.% of copper significantly suppressed formation of dendritic structure. It also led to formation of Cu-rich and Ti-rich phases in the NiTiCu matrix. Its elemental spectrum (Fig. 4.5c2) confirms this. Formation of elongated coarse grains along with porosity can be seen in the microstructure of the optimized multi-layer deposition of NiTi20Cu by T-WAAM process (Fig. 4.5d1). It is due to slow cooling rate and high heat input associated with the T-WAAM process. These grains are well-defined, indicating slower solidification rates that allow for more uniform grain growth. The Table 4.3 highlights that at.% of Ti is more than at.% of Ni in all the developed SMAs and T-WAAM developed NiTi20Cu SMA has slightly more at.% of copper than that developed by μ -PAMAM process.

4.4 Analysis of Evolution of Phases

Fig 4.6 illustrates the X-ray diffraction (XRD) graphs of the developed SMAs fabricated by μ -PAMAM and T-WAAM processes. Observed peaks in the XRD graphs were matched with the JCPDS database (00-033-0474) and (00-044-0113) to identify different phases.

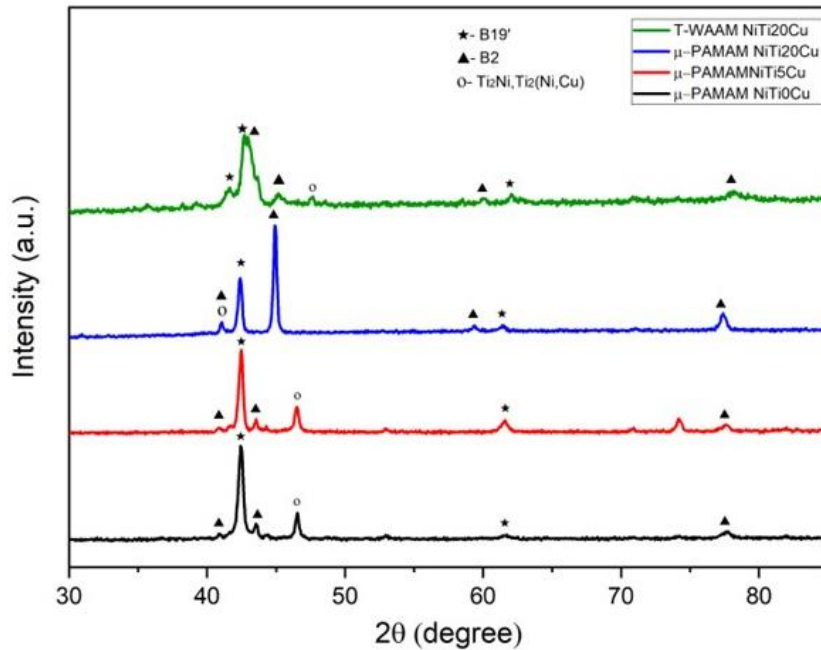
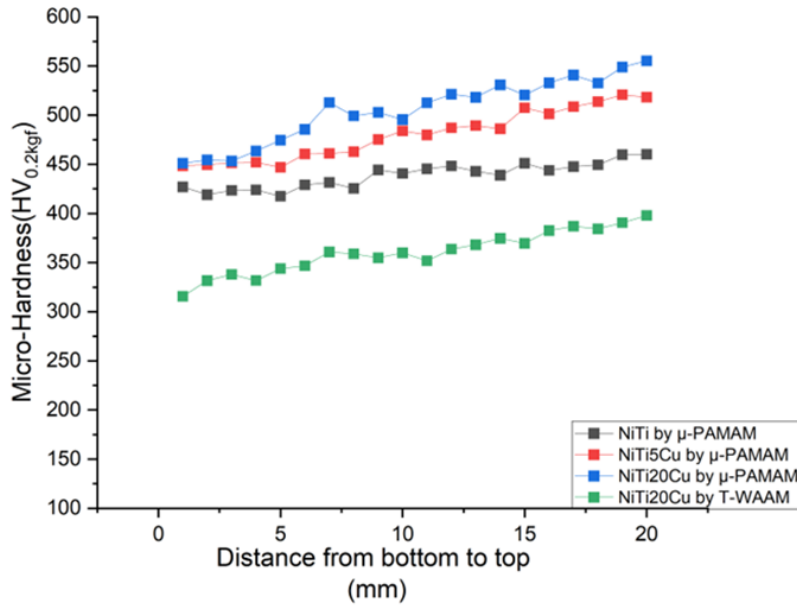


Fig. 4.6: XRD graphs for multi-layer depositions of NiTi, NiTi5Cu, and NiTi20Cu by μ -PAMAM process and NiTi20Cu by T-WAAM process.

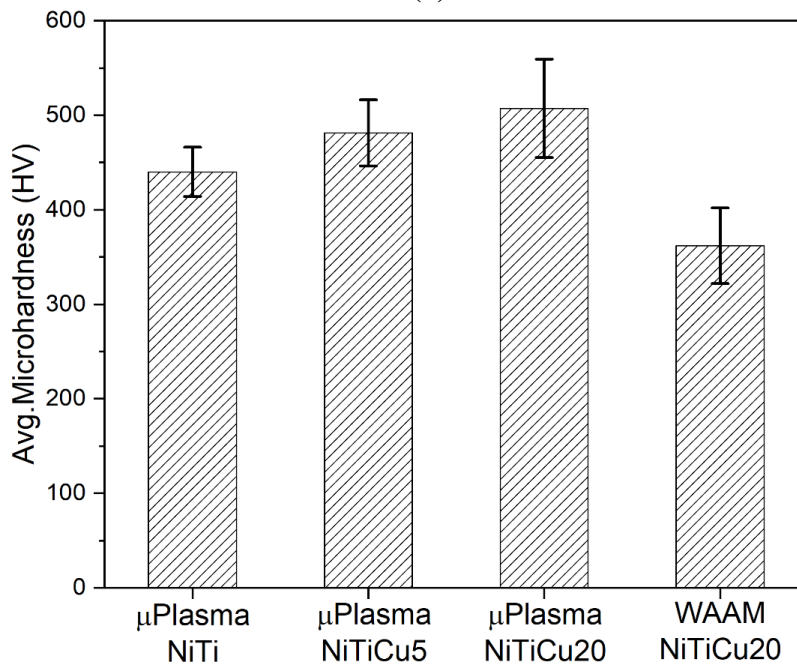
Following phases are identified in the XRD peaks in the optimized multi-layer deposition samples of NiTi, NiTi5Cu and NiTi20Cu SMA manufactured by μ -PAMAM process, and NiTi20Cu SMA manufactured by T-WAAM process: (i) austenite phase having body centred cubic (BCC) crystal structure i.e., B2 phase shown by black colour triangle, (ii) martensite phase having monoclinic crystal structure i.e., B19' phase shown by black colour star, (iii) Ti_2Ni intermetallic phase, and (iv) $Ti_2(Ni, Cu)$ intermetallic phase in the NiTiCu matrix. The B2 phase is critical for the high-temperature shape memory effect because it remains stable at the elevated temperatures and transforms to the martensitic phase upon cooling. The B19' phase is crucial for super-elasticity and the shape memory effect at lower temperatures and it reverts back to the B2 phase upon heating. The Ti_2Ni and $Ti_2(Ni, Cu)$ intermetallic phases typically constitute the secondary phases due to excess titanium which can influence the mechanical properties and phase transformation characteristics of an SMA. A notable shift in the peak of B2 phase is observed as the copper content increases. Specifically, the peaks for the B2 phase in the alloy with higher copper content (T-WAAM processed NiTi20Cu) are slightly shifted towards lower values of 2θ . These peak shifts occur due to lattice distortion caused by the substitution of nickel or titanium atoms by copper atoms in the lattice leading to changes in the lattice parameters. The difference in atomic radius between copper and Ni/Ti results in altered lattice spacing.

4.5 Microhardness Results

Fig. 4.7a shows microhardness profile of optimized multi-layer deposition of NiTi, NiTi5Cu, NiTi20Cu manufactured by μ -PAMAM process and NiTi20Cu by T-WAAM process along their build direction and Fig. 4.7b depicts their average microhardness values as 440 HV, 481.4 HV, 507.2 HV, and 361 HV respectively.



(a)



(b)

Fig. 4.7: Results of microhardness evaluation of NiTi_xCu SMAs: (a) microhardness profile along the build direction, and (b) average values of microhardness.

Following are the observations from Figs. 4.7a and 4.7a and their explanations:

- Microhardness values of all the developed SMAs gradually increases along the build direction i.e., from the bottom layer towards the top layer. It is because of slow cooling of

the previously deposited layer(s) than the top layer. It results grains of the previously deposited layer(s) getting more time to grow thus forming coarser grains and lesser microhardness value.

- The optimized multi-layer deposition of NiTi20Cu SMA developed by μ -PAMAM process has maximum value of microhardness along its build direction (Fig. 4.7a) as well as maximum value of average microhardness i.e., 507.2 HV (Fig. 4.7b). This is followed by microhardness profiles and average microhardness values for optimized multi-layer depositions of NiTi5Cu (i.e., 481.4 HV) and NiTi SMA (i.e., 440 HV) developed by μ -PAMAM process. Whereas the optimized multi-layer deposition of NiTi20Cu SMA developed by T-WAAM process has minimum value of microhardness along its build direction and minimum value of average microhardness (i.e., 361 HV). It can be explained by the following facts: (i) Addition of Cu to NiTi SMA increases microhardness of resultant SMA because copper atoms replace some atoms of nickel or titanium in the NiTi lattice causing lattice distortions. It impedes movement of dislocations, a phenomenon known as *solid solution strengthening*. Additionally, formation of fine precipitates contributes to *precipitation hardening* thus further enhancing microhardness of μ -PAMAM developed NiTi5Cu and NiTi20Cu SMAs than μ -PAMAM developed NiTi SMA, (ii) Microhardness of μ -PAMAM developed NiTi20Cu SMA is more than that of μ -PAMAM developed NiTi5Cu SMA. This is due to formation of more brittle intermetallic phases and finer precipitates with addition of more amount of copper, and (iii) T-WAAM process involves higher heat input and slow cooling which leading to coarser microstructures and uniform phase distribution which caused T-WAAM developed NiTi20Cu SMA to have minimum values of microhardness profile and average microhardness (i.e., 361 HV) among all the tested samples of SMAs.

4.6 Tensile Properties

Fig. 4.8 shows graphs between the engineering stress and engineering strain for μ -PAMAM developed optimized multi-layer deposition of NiTi SMA (Fig. 4.8a), NiTi5Cu SMA (Fig. 4.8b), and NiTi20Cu SMA (Fig. 4.8c) and T-WAAM developed optimized multi-layer deposition NiTi20Cu SMA (Fig. 4.8d) obtained from their uniaxial tensile tests. Table 4.4 presents values of ultimate tensile strength and elongation for them.

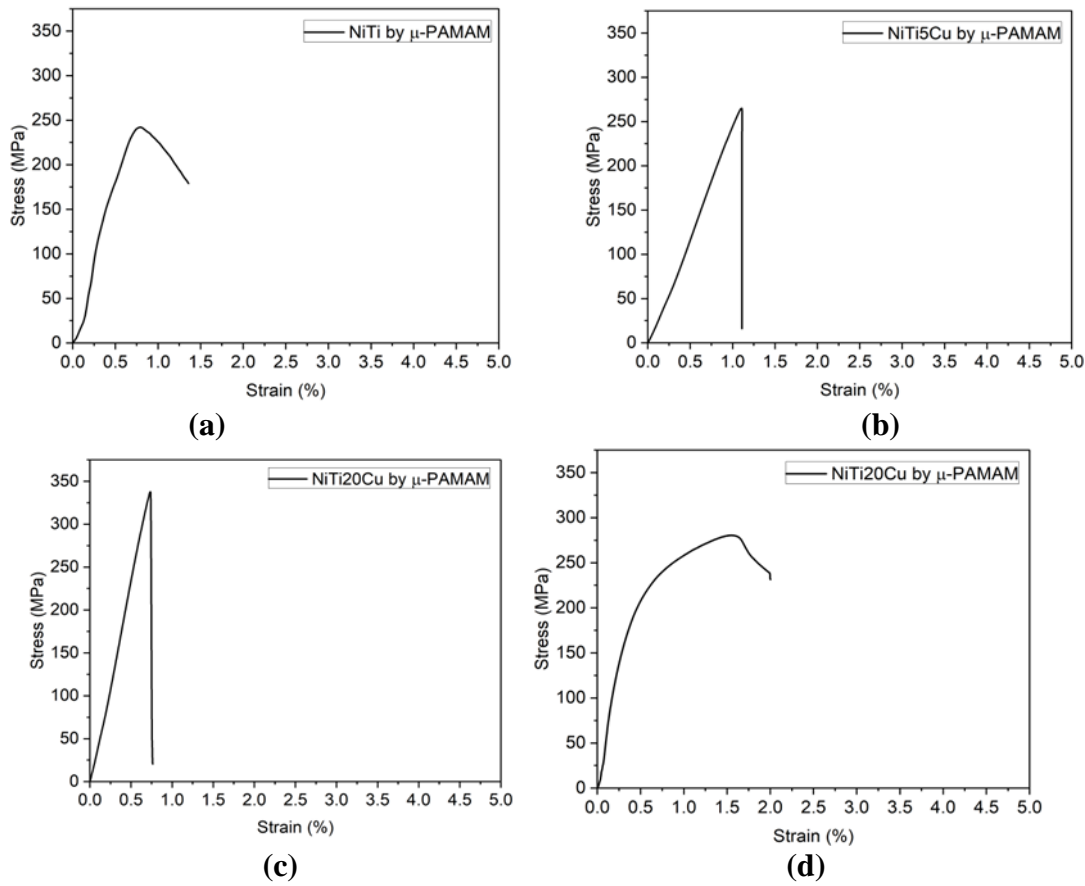


Fig. 4.8: Engineering stress and engineering strain graphs for: (a) μ -PAMAM developed NiTi SMA, (b) μ -PAMAM developed NiTi5Cu SMA, (c) μ -PAMAM developed NiTi20Cu SMA, and (d) T-WAAM developed NiTi20Cu SMA.

Table 4.4: Ultimate tensile strength (UTS) and elongation for the optimized multi-layer depositions of NiTiXCu SMAs obtained from their tensile tests.

SMA	Ultimate tensile strength (MPa)	Elongation (%)
NiTi by μ -PAMAM	236.5	1.35
NiTi-5Cu by μ -PAMAM	263.7	1.11
NiTi-20Cu by μ -PAMAM	338.5	0.76
NiTi-20Cu by T-WAAM	281.0	1.7

Following are the observations from Fig. 4.8 and Table 4.4 and their explanations:

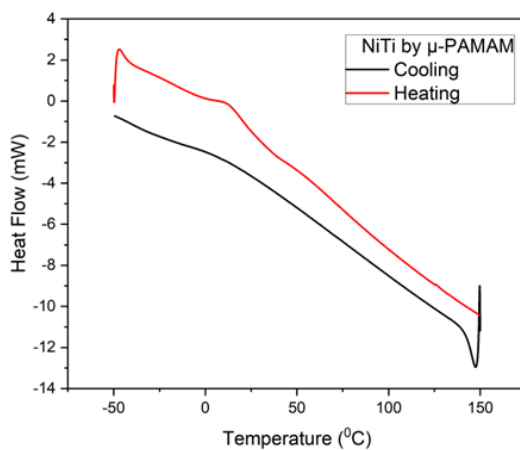
- The μ -PAMAM developed optimized multi-layer deposition of NiTi20Cu SMA has maximum value of ultimate tensile strength (i.e., 338.5 MPa) but minimum value of elongation (i.e., 0.76%) implying that this SMA does not exhibit plastic deformation before failure. Whereas, μ -PAMAM developed optimized multi-layer depositions of NiTi SMA has minimum UTS of 236.5 MPa and elongation of 1.35% and NiTi5Cu SMA has UTS of 263.7 MPa and elongation as 1.11%. It can be explained by the following facts: (a) Addition of copper improves UTS but reduces elongation i.e., ductility because it creates a solid solution in which copper atoms replace some of the nickel atoms in the

NiTi lattice. It distorts the lattice of NiTi and makes dislocation movement more difficult thereby increasing tensile strength of the resultant SMA. Presence of copper also disrupts the smooth phase transformation process of NiTi thus leading to reduced ductility and elongation, and (ii) Addition of higher copper content (20%) causes formation of brittle intermetallic phases such as Ti_2Ni or $Cu(Ti, Ni)$ and alter the phase stability of the NiTi matrix. The intermetallic phases though increase strength but reduces ductility.

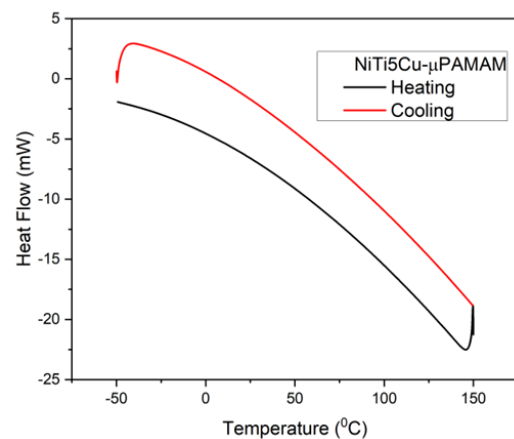
- The T-WAAM developed optimized multi-layer deposition of NiTi20Cu SMA has maximum value of elongation (i.e., 1.7%) and 2nd maximum UTS (i.e., 281 MPa) i.e., good combination of ductility and strength. Good elongation is due to slow cooling rate in T-WAAM process which results in a more uniform distribution of phases and different phase fraction thus reducing formation of brittle intermetallic compounds.

4.7 Phase Transformation Behavior

Phase transformation behaviour is a primary requirement for an SMA it confirms ability of the developed SMA to possess the SME. Differential scanning calorimetry (DSC) is used to study phase transformation behaviour of an SMA. The phase transformations occur due to the thermally induced martensitic transformation in an SMA. When an SMA is heated it absorbs heat and transforms from low-temperature martensite phase to high-temperature austenite phase thus showing an endothermic peak (i.e., upward peak in the heating curve). And, when an SMA is cooled it undergoes a transformation from the high-temperature austenite phase to low-temperature martensite phase thus releasing latent heat which is shown as an exothermic peak (downward peak in the cooling curve). Fig. 4.9 shows heating and cooling curves for μ -PAMAM developed NiTi SMA (Fig. 4.9a), NiTi5Cu SMA (Fig. 4.9b), NiTi20Cu SMA (Fig. 4.9c), and for T-WAAM developed NiTi20Cu SMA (Fig. 4.9d) obtained from their DSC.



(a)



(b)

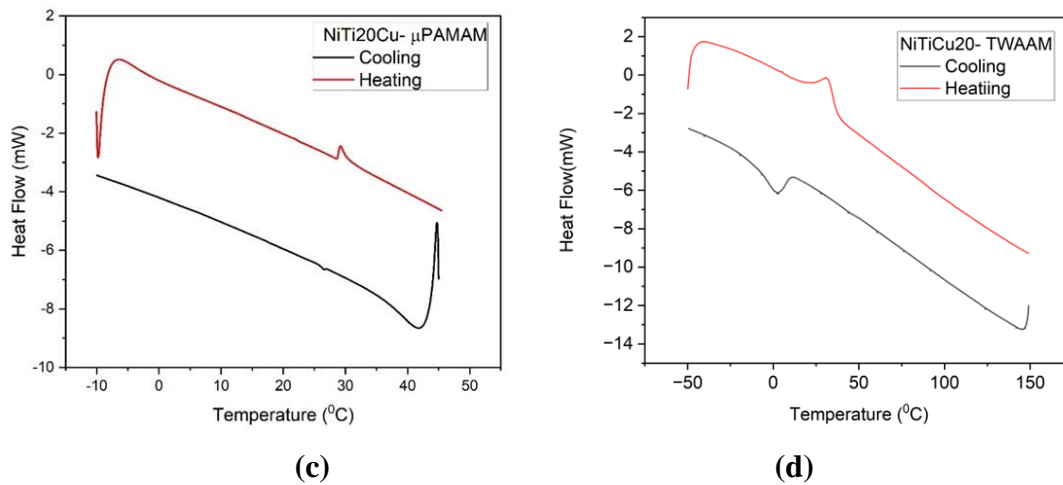


Fig. 4.9: Phase transformation pattern of NiTi_xCu alloys: (a) NiTi, (b) NiTi5Cu, (c) NiTi20Cu by μ -PAMAM process and (d) NiTi20Cu by T-WAAM process.

Following are the observations from Fig. 4.9 and their explanations:

- The μ -PAMAM developed NiTi SMA shows a visible peak in its heating curve but does not display any peak in its cooling curve (Fig. 4.9a) whereas μ -PAMAM developed NiTi5Cu SMA does not show any peak in its heating and cooling curves (Fig. 4.9b).
- The μ -PAMAM developed NiTi20Cu SMA shows the martensite start temperature ' M_s ' as 26.96 °C, martensite finish temperature ' M_f ' as 25.65°C, austenite start temperature ' A_s ' as 28.65°C, and austenite finish temperature ' A_f ' as 31.21°C (Fig. 4.9c). The T-WAAM developed NiTi20Cu SMA depicts the martensite start temperature ' M_s ' as 10.7°C, martensite finish temperature ' M_f ' as -5.06°C, austenite start temperature ' A_s ' as 18.1°C, and austenite finish temperature ' A_f ' as 39.1°C. This can be explained by following facts: (i) Addition of sufficient amount of copper to NiTi SMA influences phase transformation temperatures because copper atoms substitute for some nickel atoms in the NiTi matrix which changes the lattice structure and affects the stability of the phases. This results in different start and finish temperatures for the martensitic and austenitic phases, (ii) Such substitution distorts the lattice distortions due to their different atomic sizes and such lattice distortions reduce start and finish temperatures of martensite and austenite phases.
- The μ -PAMAM developed NiTi20Cu SMA has hysteresis of 4.25°C (i.e., temperature difference between austenite finish temperature ' A_f ' and martensite start temperature ' M_s ') whereas T-WAAM developed NiTi20Cu SMA shows hysteresis of 28.4°C. It implies that addition of copper to NiTi SMA reduced the thermal hysteresis. It is because copper tends to stabilize the austenite phase resulting in sharper and more distinct transformation peaks in the DSC curves.

This chapter presents the results for the single-layer depositions of NiTi, NiTi5Cu and NiTi20 Cu SMA fabricated by μ -PAMAM process during the main experiments and single-layer depositions of NiTi20Cu manufactured by T-WAAM process along with results for their optimized multi-layer depositions. It also presents results and analysis of aspect ratio and dilution for the single-layer depositions of the developed SMAs, and analysis of microstructure, formation of phases, tensile properties, microhardness, and phase transformation behaviour for optimized multi-layer depositions. The *next and last chapter* presents significant achievements and conclusions of the present work along with some directions for the future research.

Chapter 5

Conclusions and Scope for Future Work

5.1 Significant Achievements

Following worth-mentioning significant achievements of the present work:

- Development of optimized multi-layer deposition (consisting of 8 layers) of NiTi, NiTi5Cu, and NiTi20Cu SMAs by μ -PAMAM process using feedstock material in powder form
- Development of 15 mm wide optimized multi-layer deposition (consisting of 12 layers) of NiTi20Cu SMA by T-WAAM process using wires of NiTi and Cu
- Achieved thermal hysteresis of 4.25°C for NiTi20Cu developed by μ -PAMAM process.

5.2 Conclusions

This work investigated on the development of NiTi, NiTi5Cu, and NiTi20Cu SMAs by μ -PAMAM process and NiTi20Cu SMA by T-WAAM process, their characterization and comparative study. The primary objective was to understand the effects of adding copper to NiTi SMA on the microstructure, mechanical properties, and phase transformation behavior of the resultant SMAs. Following are the major conclusions that can be drawn from the present work:

- Microstructure of NiTi and NiTi5Cu SMAs developed by μ -PAMAM process primarily consists of columnar dendritic structure with formation of Ti-rich phase in the dendritic regions. Addition of 5 at.% copper led to formation of Cu (Ni, Ti) phase suggesting some degree of Cu segregation, altering the segregation pattern of Ni and Ti during the solidification, and formation of Cu-containing intermetallic phase. Addition of 20at.% of copper to NiTi significantly suppressed formation of dendritic structure and led to formation of Cu-rich and Ti-rich phases in the NiTiCu matrix. Microstructure of NiTi20Cu SMA developed by T-WAAM process consists of some porosity and elongated well-defined coarse grains with indicating slower solidification rate that allow for more uniform grain growth. The at.% of Ti is more than at.% of Ni in all the developed SMAs and T-WAAM developed NiTi20Cu SMA has slightly more at.% of copper than that developed by μ -PAMAM process.
- The developed SMAs contained austenite or B2 phase having BCC crystal structure, martensite or B19' phase having monoclinic crystal structure, Ti2Ni intermetallic phase, and Ti2(Ni, Cu) intermetallic phase in the NiTiCu matrix. The B2 phase is critical for the high-temperature shape memory effect because it remains stable at the elevated temperatures and transforms to the martensitic phase upon cooling and B19' phase is

crucial for super-elasticity and the shape memory effect at lower temperatures and it reverts back to the B2 phase upon heating. The Ti₂Ni and Ti₂(Ni, Cu) intermetallic phases typically constitute the secondary phases due to excess titanium which can influence the mechanical properties and phase transformation characteristics of an SMA. A notable shift in the peak of B2 phase is observed as the copper content increases due to lattice distortion caused by the substitution of Ni or Ti atoms by Cu atoms in the lattice.

- The NiTi₂₀Cu SMA developed by μ -PAMAM process has maximum value of microhardness along its build direction as well as maximum value of average microhardness as 507.2 HV. This is followed by microhardness profiles and average microhardness values of μ -PAMAM developed NiTi₅Cu and NiTi SMA as 481.4 HV and 440 HV respectively. Whereas, NiTi₂₀Cu SMA developed by T-WAAM process has minimum value of microhardness along its build direction and minimum value of average microhardness of 361 HV.
- The μ -PAMAM developed NiTi₂₀Cu SMA has maximum ultimate tensile strength (i.e., 338.5 MPa) but minimum elongation (i.e., 0.76%) whereas, NiTi SMA has minimum UTS of 236.5 MPa and elongation of 1.35% and NiTi₅Cu SMA has UTS of 263.7 MPa and elongation as 1.11%. This implies that addition of Cu to NiTi SMA improves tensile strength but reduces ductility. The T-WAAM developed NiTi₂₀Cu SMA has maximum value of elongation i.e., 1.7% and 2nd maximum tensile strength UTS (i.e., 281 MPa). This good combination of ductility and strength is due to slow cooling rate in T-WAAM process which results in a more uniform distribution of phases and different phase fraction thus reducing formation of brittle intermetallic compounds.
- The μ -PAMAM developed NiTi SMA shows a visible peak in its heating curve but does not display any peak in its cooling curve whereas μ -PAMAM developed NiTi₅Cu SMA does not show any peak in its heating and cooling curves. But, μ -PAMAM developed NiTi₂₀Cu SMA shows martensite start temperature ' M_s ' as 26.96 °C, martensite finish temperature ' M_f ' as 25.65°C, austenite start temperature ' A_s ' as 28.65°C, and austenite finish temperature ' A_f ' as 31.21°C (Fig. 4.9c). The T-WAAM developed NiTi₂₀Cu SMA showed these values as 10.7°C, -5.06°C, 18.1°C, and 39.1°C respectively. It implies that adding sufficient amount of Cu to NiTi SMA influences phase transformation temperatures due to substitution of some Ni atoms in the NiTi matrix by Cu atoms thus affecting stability of the phases and different start and finish temperatures for the martensitic and austenitic phases. Substitution of Ni atoms by Cu atoms distorts the lattice due to their different atomic sizes. This distortion reduces start and finish temperatures of martensite and austenite phases.

- This study demonstrated that addition of copper to NiTi SMA significantly reduced the hysteresis temperature (i.e., μ -PAMAM developed NiTi₂₀Cu SMA has hysteresis of 4.25°C) due Cu tendency to stabilize austenite phase resulting in sharper and more distinct transformation peaks in the DSC curve. It will enhance performance of the resultant SMAs in the application that require precise thermal responses.
- The finding from this research work provides valuable insights into the AM of SMAs and benefits of adding Cu to NiTi SMA. These insights will give the way for future research and development in SMA applications particularly in the fields requiring high reliability and precise actuation such an aerospace, biomedical devices, and robotics.

5.3 Scope for Future Work

- Different amount of copper can be added to find its upper limit for development of NiTi_xCu SMAs
- Study of wear characteristics and corrosion behavior of the developed NiTi_xCu SMAs to make usable for marine and aerospace applications.
- Development of some useful components from the developed SMAs for some real-world applications.

References

- Alijani, F., Ahmed, R., Mohammad, G., Morteza, A. Ali K.O. 2014.** “Effect of milling time on the structure, micro-hardness, and thermal behavior of amorphous/nanocrystalline TiNiCu shape memory alloys developed by mechanical alloying” *Materials & Design* 55, 373–380. <https://doi.org/10.1016/j.matdes.2013.09.009>
- Andrianesis, K., Tzes, A., Kolyvas, E., Koveos, Y. 2007.** “Development and control of an ultra-lightweight anthropomorphic modular finger actuated by shape memory alloy wires” *Proceedings of the 15th Mediterranean Conference on Control & Automation*, .
- Araújo, C.J., da Silva, N.J., da Silva M.M., Gonzalez, C.H. 2011.** “A comparative study of Ni-Ti and Ni-Ti-Cu shape memory alloy processed by plasma melting and injection molding” *Materials & Design* 32(10), 4925-4930. <https://doi.org/10.1016/j.matdes.2011.05.051>
- Arya, P.K., Jain, N.K., Sathiaraj, D., Patel, V. 2024,** “Development of high strength and lightweight Ti6Al4V5Cr alloy: Microstructure and mechanical characteristics” *Journal of Materials Research and Technology*, 28, 3526-3540 <https://doi.org/10.1016/j.jmrt.2023.12.271>
- Bram, M., Ahmad-Khanlou, A., Heckmann, A., Fuchs, B., Buchkremer, H., Stöver, D., 2002.** “Powder metallurgical fabrication processes for NiTi shape memory alloy parts” *Materials Science and Engineering: A* 337(1-2), 254–263. [https://doi.org/10.1016/S0921-5093\(02\)00028-X](https://doi.org/10.1016/S0921-5093(02)00028-X)
- Cai, M., Fu Y.Q., Sanjabi, S., Barber, Z.H., Dickinson, J.T. 2007.** “Effect of composition on surface relief morphology in TiNiCu thin films” *Surface and Coatings Technology* 201(12), 5843–5849. <https://doi.org/10.1016/j.surfcoat.2006.10.033>
- Chen, G., Ma, Y., Teng, X., Liu, J., Zhang, B., Cao, J., Huang, J. 2023.** “Microstructure evolution and shape memory function mechanism of NiTi alloy by electron beam 4D printing” *Applied Materials Today* 31, 101749. <https://doi.org/10.1016/j.apmt.2023.101749>
- Cheng, X., Huang, F., Li, N., Wu, X. 2008.** “Microstructure and shape memory effect of Cu-26.1Zn-4.8Al alloy” *Journal of Wuhan University of Technology-Mater. Sci. Ed.* 23(5), 717–19. <https://doi.org/10.1007/s11595-007-5717-7>
- Cirstea, C.D., Cirstea, V., Marinescu, V., Patroi, D., Tiganescu, T.V. 2023.** The Microstructure influence on mechanical properties of Ti₅₀Ni_{50-x}Cu_x materials achieved by spark plasma sintering at 800–900°C, *Romanian Journal of Physics*, 68, 615. https://rjp.nipne.ro/2023_68_5-6/RomJPhys.68.615.pdf
- Dutkiewicz, J., Rogal, L. Kalita, D., Węglowski, M., Błacha, S., Berent, K., Czeppe, T., A Dudka, A.A, Durejko, T., Czujko, T. 2020.** “Superelastic effect in NiTi alloys manufactured using electron beam and focused laser rapid manufacturing methods” *Journal of Materials Engineering and Performance* 29(7), 4463–4473. <https://doi.org/10.1007/s11665-020-04938-z>

- Fink, A., Fu, Z., Körner, C. 2023.** “Functional properties and shape memory effect of nitinol manufactured via electron beam powder bed fusion” *Materialia* 30, 101823.
<https://doi.org/10.1016/j.mtla.2023.101823>
- Fu, B., Feng, K., Li, Z. 2018.** “Study on the effect of Cu addition on the microstructure and properties of NiTi alloy fabricated by laser cladding” *Materials Letters* 220, 148–151.
<https://doi.org/10.1016/j.matlet.2018.03.030>
- Gao, S., Weng, F., Bodunde, O., Qin, M., Liao, W., Guo, P. 2021.** “Spatial characteristics of nickel-titanium shape memory alloy fabricated by continuous directed energy deposition” *Journal of Manufacturing Processes* 71, 417–428.
<https://doi.org/10.1016/j.jmapro.2021.09.039>
- Goryczka, T., Karolus, M., Ochinn, P., Morawiec, H. 2001.** “Structure of melt spun Ni₂₅Ti₅₀Cu₂₅ ribbons studied by X-ray diffraction.” *Le Journal de Physique IV* 11 (PR8): Pr8-345-Pr8-350. <https://doi.org/10.1051/jp4:2001858>
- Goryczka, T., Humbeeck, J. 2008.** “NiTiCu shape memory alloy produced by powder technology” *Journal of Alloys and Compounds* 456(1–2), 194–200.
<https://doi.org/10.1016/j.jallcom.2007.02.094>
- Gu, H.D., Leung, K. M., Chung, C. Y., 1998.** “Growth of high-temperature NiTi_{1-x}Hf_x shape memory alloy thin films by laser ablation of composite targets” *Journal of Vacuum Science & Technology A: Vacuum, Surfaces, and Films* 16(6), 3420–3422.
<https://doi.org/10.1116/1.581496>
- Hassdorf, R., Feydt, J., Pascal, R., Thienhaus, S., Boese, M., Sterzl, T., Winzek, B., Moske, M. 2002.** “Phase formation and structural sequence of highly-oriented MBE-grown NiTiCu shape memory thin films” *Materials Transactions* 43(5), 933–38.
<https://doi.org/10.2320/matertrans.43.933>
- Krishna, B.V., Bose, S., Bandyopadhyay, A. 2007.** “Laser processing of net-shape NiTi shape memory alloy.” *Metallurgical and Materials Transactions A* 38(5), 1096–1103.
<https://doi.org/10.1007/s11661-007-9127-4>
- Kubášová, K., Drátovská, V., Losertová M., Salvetr, P., Kopelent, M., Kořínek, F., Havlas, H., Džugan, J., Daniel, M. 2024.** “A review on additive manufacturing methods for NiTi shape memory alloy production.” *Materials* 17(6), 1248.
<https://doi.org/10.3390/ma17061248>
- Sujith, K.S., Marandi, L., Balla, V.K., Bysakh, S., Piorunek, D. Eggeler, G., Das, M. Sen, I. 2019.** “Microstructure-property correlations for additively manufactured NiTi based shape memory alloys” *Materialia* 8, 100456.
<https://doi.org/10.1016/j.mtla.2019.100456>
- Liang, C. 1990.** “The constitutive modeling of shape memory alloys” PhD Thesis, Virginia Polytechnic Institute and State University, <http://hdl.handle.net/10919/39218>
- Liu, G., Zhou, S., Lin, P., Zong,X., Chen, X., Zhang, Z., Ren, L. 2022.** “Analysis of microstructure, mechanical properties, and wear performance of NiTi alloy fabricated by cold metal transfer based wire arc additive manufacturing” *Journal of Materials Research and Technology* 20, 246–259 <https://doi.org/10.1016/j.jmrt.2022.07.068>

- Locci, A.M., Orrù, R., Cao, G., Munir, Z. A. 2003.** “Field-activated pressure-assisted synthesis of NiTi” *Intermetallics* 11 (6): 555–71. [https://doi.org/10.1016/S0966-9795\(03\)00043-8](https://doi.org/10.1016/S0966-9795(03)00043-8)
- Lu, B., Cui, X., Liu, E., Feng, X., Dong, M., Li, Y., Wang, H., Jin, G. 2018.** “Influence of microstructure on phase transformation behavior and mechanical properties of plasma arc deposited shape memory alloy” *Materials Science and Engineering: A* 736, 130–136. <https://doi.org/10.1016/j.msea.2018.08.098>
- Lv, H., Leng, J., Liu, Y., Du, S. 2008.** “Shape-memory polymer in response to solution.” *Advanced Engineering Materials* 10(6), 592-595. <https://doi.org/10.1002/adem.200800002>
- Mineta, T., Deguchi, T., Makino, E., Kawashima, T., Shibata, T. 2011.** “Fabrication of cylindrical micro-actuator by etching of TiNiCu shape memory alloy tube” *Sensors and Actuators A: Physical* 165(2), 392–398. <https://doi.org/10.1016/j.sna.2010.12.002>
- Moberly, Warren J., Melton, K.N. 1990.** “Ni-Ti-Cu shape memory alloys.” in *Engineering Aspects of Shape Memory Alloys*, 46–57. Elsevier. <https://doi.org/10.1016/B978-0-7506-1009-4.50008-1>
- Mohd Jani, J., Leary, M., Subic, A., Gibson, A. 2014.** “A review of shape memory alloy research, applications and opportunities” *Materials & Design*, 56, 1078–1113. <https://doi.org/10.1016/j.matdes.2013.11.084>
- Morris, D.G., Morris, M.A., 1989.** “NiTi intermetallic by mixing, milling and interdiffusion elemental components”. *Materials Science and Engineering: A*, 110, pp.139-149. [https://doi.org/10.1016/0921-5093\(89\)90165-2](https://doi.org/10.1016/0921-5093(89)90165-2)
- Peng, X., Pi, W., Fan, J. 2008.** “A microstructure-based constitutive model for the pseudoelastic behavior of NiTi SMAs” *International Journal of Plasticity* 24(6), 966–990. <https://doi.org/10.1016/j.ijplas.2007.08.003>
- Pons, J.L. 2005.** “*Emerging Actuator Technologies: a Micromechatronic Approach*”, John Wiley & Sons, New Jersey, ISBN: 978-0-470-09199-9.
- Pu, Z., Du, D., Wang, K., Liu, G., Zhang, D., Wang, X., 2021.** “Microstructure, phase transformation behavior and tensile superelasticity of NiTi shape memory alloys fabricated by the wire-based vacuum additive manufacturing” *Materials Science and Engineering: A* 812, 141077. <https://doi.org/10.1016/j.msea.2021.141077>
- Raza, Syed A., Muhammad I. K., Mairaj A., Danish, T., Asim, I., Rida, B.N 2021.** “Effect of nano-silica volume reinforcement on the microstructure, mechanical, phase distribution and electrochemical behaviour of pre-alloyed titanium-nickel (Ti-Ni) powder.” *Key Engineering Materials* 875, 60–69. <https://doi.org/10.4028/www.scientific.net/KEM.875.60>
- Resnina, N., Palani, I.A., Belyaev, S., Prabu, S.S.M., Liulchak, P.z Karaseva, U., Manikandan M., et al. 2021a.** “Structure, martensitic transformations and mechanical behaviour of NiTi shape memory alloy produced by wire arc additive manufacturing” *Journal of Alloys and Compounds* 851, 156851 <https://doi.org/10.1016/j.jallcom.2020.156851>

- Resnina, N., Palani, I.A., Belyaev, S., Singh, S., Liulchak, P., Karaseva, U., Prabu, S.S.M., et al. 2021b.** “Influence of heat treatment on the structure and martensitic transformation in NiTi alloy produced by wire arc additive manufacturing.” *Materialia* 20, 01238. <https://doi.org/10.1016/j.mtla.2021.101238>
- Ron, T., Amnon S., Eli, A. 2023.** “Additive manufacturing technologies of high entropy alloys (HEA): review and prospects” *Materials* 16(6), 2454. <https://doi.org/10.3390/ma16062454>
- Salman, K.D. 2021.** “Manufacture of shape memory alloys NiTi and NiTiCu by casting method and studying the effect of adding the copper element in different proportions to the binary alloy on the microstructure, phase transformations and conductivity” *Journal of Physics: Conference Series* 1973(1), 012108. <https://doi.org/10.1088/1742-6596/1973/1/012108>
- Santosh, S, Sampath, V. 2020.** “Experimental investigations on the effect of copper on the microstructure and shape memory characteristics of NiTi alloys” *IOP Conference Series: Materials Science and Engineering* 912(5), 052009. <https://doi.org/10.1088/1757-899X/912/5/052009>
- Shiva, S., Palani, I.A., Mishra, S.K., Paul, C.P., Kukreja, L.M. 2016.** Influence of Cu addition to improve shape memory properties in NiTi alloys developed by laser rapid manufacturing. *Journal of Laser Micro Nanoengineering*, 11(2), 153. <https://doi.org/10.2961/jlmn.2016.02.0003>
- Singh, S., Palani, I.A., Shirin D., Paul, C.P., Prashanth, K.G., Qureshi, A.J. 2023.** “Influence of the interlayer temperature on structure and properties of CMT wire arc additive manufactured NiTi structures” *Journal of Alloys and Compounds* 966, 171447. <https://doi.org/10.1016/j.jallcom.2023.171447>
- Tadaki, T., Otsuka, K., Shimizu, K. 1988.** “Shape memory alloys.” *Annual Review of Materials Science* 18(1), 25-45. <https://doi.org/10.1146/annurev.ms.18.080188.000325>
- Valeanu, M., Lucaci, M., Crisan, A. D., Sofronie, M., Leonat, L., Kuncser, V., 2011.** “Martensitic transformation of Ti50Ni30Cu20 alloy prepared by powder metallurgy” *Journal of Alloys and Compounds* 509(13), 4495–4498. <https://doi.org/10.1016/j.jallcom.2011.01.154>
- Velmurugan, C., Senthilkumar. V. 2018.** “The effect of cu addition on the morphological, structural and mechanical characteristics of nanocrystalline NiTi shape memory alloys” *Journal of Alloys and Compounds* 767, 944–954. <https://doi.org/10.1016/j.jallcom.2018.07.217>
- Wang, C., Tan, X.P., Du, Z., Chandra, S., Sun, Z., Lim, C.W.J., Tor, S.B, Lim, C.S., Wong, C.H. 2019.** “Additive manufacturing of NiTi shape memory alloys using pre-mixed powders.” *Journal of Materials Processing Technology* 271, 152–161. <https://doi.org/10.1016/j.jmatprotec.2019.03.025>
- Wen, Jie, S., Fei, G., Yan, L., Yan, Z., Shi Y. 2021.** “Research status and prospect of additive manufactured nickel-titanium shape memory alloys” *Materials* 14(16), 4496. <https://doi.org/10.3390/ma14164496>

- Zhang**, Wei, J., Xiaobing, C., Kazuhiro, R., Makoto, A. **1999**. “The nature of reversible change in temperatures of TiNi alloys with alternating aging” *Materials Transactions, JIM* 40(12), 1367–1375. <https://doi.org/10.2320/matertrans1989.40.1367>
- Zheng**, D., Rui, D.L., Yuan, T.C., Xiong, Y. Song, B., Wang, Z.X., Su, Y.D. **2021**. “Microstructure and mechanical property of additively manufactured NiTi alloys: a comparison between selective laser melting and directed energy deposition” *Journal of Central South University* 28(4), 1028–1042. <https://doi.org/10.1007/s11771-021-4677-y>
- Zheng**, Y., Li, L., Cui. **2009**. “Repeatable temperature memory effect of TiNi shape memory alloys.” *Materials Letters* 63(11), 949–951. <https://doi.org/10.1016/j.matlet.2009.01.069>